mathematics

MDPI

Article

Pinning Event-Triggered Scheme for Synchronization of Delayed Uncertain Memristive Neural Networks

Jiejie Fan [1,2], Xiaojuan Ban [1,2,3,*,†], Manman Yuan [4,5,*,†] and Wenxing Zhang [6,7]

[1] Beijing Advanced Innovation Center for Materials Genome Engineering, University of Science and Technology Beijing, Beijing 100083, China; jjf@ustb.edu.cn
[2] School of Intelligence Science and Technology, University of Science and Technology Beijing, Beijing 100083, China
[3] Key Laboratory of Intelligent Bionic Unmanned Systems, Ministry of Education, University of Science and Technology Beijing, Beijing 100083, China
[4] School of Computer Science, Inner Mongolia University, Hohhot 010021, China
[5] National & Local Joint Engineering Research Center of Intelligent Information Processing Technology for Mongolian, Hohhot 010021, China
[6] School of Mechanical Engineering, University of Science and Technology Beijing, Beijing 100083, China; manifold@imust.edu.cn
[7] School of Mechanical Engineering, Inner Mongolia University of Science and Technology, Baotou 014010, China
* Correspondence: banxj@ustb.edu.cn (X.B.); yuanman@imu.edu.cn (M.Y.)
† These authors contributed equally to this work.

Abstract: To reduce the communication and computation overhead of neural networks, a novel pinning event-triggered scheme (PETS) is developed in this paper, which enables pinning synchronization of uncertain coupled memristive neural networks (CMNNs) under limited resources. Time-varying delays, uncertainties, and mismatched parameters are all considered, which makes the system more interpretable. In addition, from the low energy cost point of view, an algorithm for pinned node selection is designed to further investigate the newly event-triggered function under limited communication resources. Meanwhile, based on the PETS and following the Lyapunov functional method, sufficient conditions for the pinning exponential stability of the proposed coupled error system are formulated, and the analysis of the self-triggered method shows that our method can efficiently avoid Zeno behavior under the newly determined triggered conditions, which contribute to better PETS performance. Extensive experiments demonstrate that the PETS significantly outperforms the existing schemes in terms of solution quality.

Keywords: event-triggered mechanism; memristor; Zeno behavior; synchronization; pinning control

MSC: 93C10

Citation: Fan, J.; Ban, X.; Yuan, M.; Zhang, W. Pinning Event-Triggered Scheme for Synchronization of Delayed Uncertain Memristive Neural Networks. *Mathematics* **2024**, *12*, 821. https://doi.org/10.3390/math12060821

Academic Editor: Leonid Piterbarg

Received: 30 January 2024
Revised: 4 March 2024
Accepted: 5 March 2024
Published: 11 March 2024

1. Introduction

In the past decades, the control and synchronization of coupled memristive neural networks (CMNNs) have attracted attention from research science and engineering fields [1]. This is partly because the memristor can simulate the synapses of biological neurons better than the resistance. From the biological point of view, CMNNs can better describe the function of the human brain and the process of information transmission than traditional neural networks [2]. Because of this, the synchronization of CMNNs can be applied to secure communication [3], social networks [4], image protection [5], multiplex networks [6], etc. For many biological and artificial intelligence systems, the dynamical behaviors of CMNNs are significant. Meanwhile, investigating the synchronization and control of CMNNs can help to reveal the structure of the human brain nervous system and extend it to the field of artificial intelligence [7].

It should be noted that network synchronization is usually achieved by controlling all nodes of the network. However, CMNNs are often required to realize synchronization with a limited resource. In this case, it is costly and difficult to control all nodes in practical applications. Therefore, pinning control in CMNNs has become a hotspot in theoretical studies and practical applications [8–10].

Recently, various pinning control mechanisms have been proposed for different neural networks [11–13]. Wang et al. [11] designed an adaptive pinning controller for complex-valued time-varying bidirectional associative memory neural networks (BAMNNs). Yu et al. [12] investigated the pinning synchronization of inertial neural networks with complex-valued time-varying characteristics under a fixed-time interval. In addition, Zhou et al. [13] designed the event-triggered pinning control scheme, which realizes the cluster synchronization for specific coupled neural networks under Lévy noises. However, most of these control methods are based on the application of the pinning controller with continuous feedback input as time changes.

Moreover, such a pinning scheme cannot meet the requirements of practical applications under a limited network bandwidth, especially for mechanisms mimicking the human brain. In practice, many nonidentical characteristics cannot be avoided, e.g., mismatched parameters and structural instability caused by random perturbation of internal faults [14,15]. Currently, the time-varying delays and uncertain factors in chaotic neural networks are rarely discussed in the pinning synchronization of CMNNs. Therefore, it is significant to investigate these issues for CMNNs [16]. Further, the continuous communication among the nodes is an essential condition for synchronization in the above-mentioned literature, i.e., scholars usually employ a continuous feedback control method. The event-triggered mechanism is different from the traditional time-triggered mechanism in that the controller sends data only when the trigger condition is satisfied, which can save resources and reduce the update frequency of the controller. As a result, such a control method avoids unnecessary use of communication resources and network bandwidth [17]. Current instantaneous CMNN states are taken as triggering conditions by many previous event-triggered schemes, but they do not consider the uncertain factors in the information exchange process; that is, the triggered condition is not related to any uncertain factors and coupling conditions. In addition, in the existing schemes, much event-triggered control uses the fixed parameters and the time-varying delays of the system. Zhou et al. [18] established a new self-triggered control scheme to tackle pinning synchronization in the case of delayed complex networks. Zhang et al. [19] established an efficient event-triggered sampling control scheme for synchronization of T–S fuzzy complex systems. Wang et al. [20] developed a fuzzy pinning adaptive event-triggered control scheme for complex neural networks.

However, it has been proven that uncertain factors and mismatched parameters that are destructive in dynamic behaviors [21,22], often lead to desynchronization, oscillatory behaviors, or even instability. To handle such negative factors, new practical pinning control mechanisms have been designed for event-triggered schemes to improve the synchronization or stability of CMNNs. Furthermore, the new appropriate triggered condition and the Lyapunov function of the pinning schemes should be considered. In this regard, it is imperative and significant to study the exponential synchronization issue with the pinning event-triggered scheme (PETS) for CMNNs under time-varying uncertain factors. The contributions of our work are summarized below.

(1) Different from general CMNNs, the proposed model considers the time-varying uncertain factors and belongs to an uncertain switching system, which is conducive to studying the dynamic behavior of the system under different communication situations. Taking the superiority of both event-triggered control and pinning schemes, a fresh pinning event-triggered scheme is proposed, which contains the characteristics of pinning and impulsive control simultaneously to decrease the control cost-effectively.
(2) To clarify the issue of the pinning synchronization for the event-triggered scheme, an algorithm (Algorithm 1) is designed to identify the number of nodes that need to be pinned in the CMNNs. Considering the essentials of the PETS, the designed triggered

function shows the relationship between the degree of nodes, coupling matrix, and triggered instants.

(3) By designing a fresh Lyapunov functionality and adopting some inequality techniques, sufficient criteria for pinning event/self-triggered synchronization of CMNNs are obtained. It is evidenced that a higher connection degree of the pinned nodes can contribute to better performance under the PETS for the more complex coupled system. Meanwhile, the controller updates of each pinned node are driven by properly defined events, and they only depend on the combinational triggered condition. Thus, the proposed model achieves more practical results than some advanced works.

As for the rest of this paper, Section 2 introduces the model of CMNNs and the involved definitions and assumptions, as well as lemmas. Then, in Section 3, the theoretical analysis results of this paper are presented, including a theorem and two corollaries. Numerical examples are given in Section 4 to validate the main results. Section 5 draws together the main conclusions of this paper.

Notations: $\boldsymbol{C}\Big([-r,0],\mathbb{R}^n\Big)(r>0)$ in this paper denotes the Banach space of all continuous functions mapping from $[-r,0]$ to $\mathbb{R}^n$ with q-norm or ∞-norm, $\mathbb{R}^n$ denotes an Euclidean space of n dimensions, and the superscript T denotes a vector transposition or matrix transposition. In this paper, the vector norm is defined as $\|x_i\|$, which means the 2-norm of a vector x_i; $\|x_i\| = (\sum_{i=1}^{n} x_i^2)^{\frac{1}{2}}$, $co[a,b]$ refers to the closure (convex hull) of $\{a,b\}$; and $\lambda_{\max}(P)$ represents the maximum eigenvalue of matrix P.

Algorithm 1 Algorithm for self-triggered scheme

Require: $t=t_0$,$k\in N_+$,$t_{k-1}=t_0$
Ensure: $\lambda_{\max}(D^+)$,$\lambda_{\max}(A^+)$,$\lambda_{\max}(B^+)$,Y_1,Y_2

for i,j to n, and p to N **do**
  // Determine $\lambda_{\max}(D^+)$,$\lambda_{\max}(A^+)$,$\lambda_{\max}(B^+)$ by (2) concerning initial values $x(t_0)$ and $y(t_0)$;
end for
// Denote $\epsilon(t)=\epsilon(t_{k-1})$
while $t<T$, // T is the complete time of the whole system. **do**
  for i,j to n, and p to N **do**
    // Determine $\lambda_{\max}(D^+)$,$\lambda_{\max}(A^+)$,$\lambda_{\max}(B^+)$ by (2) concerning $x(t_{k-1})$ and $y(t_{k-1})$;
  end for
  // Compute Y_1,Y_2,
  // $\tilde{t}_k=\tilde{t}_{k-1}+\frac{1}{\mathrm{Y}_2}\ln\Big(1+\frac{\mathrm{Y}_2}{\mathrm{Y}_1}\sqrt{\hbar(\epsilon(t))}\Big)$
  if $t=\tilde{t}_k$ // which means the system is triggered. **then**
    // Update $k=k+1$; $t_{k-1}=t$; $\epsilon(t)=\epsilon(t_{k-1})$
  end if
end while

2. Preliminaries of the Neural Network Model

Here, the neural network model is first elaborated, and then the error systems and the lemmas involved in the model are provided.

2.1. The Dynamic Model of CMNNs

According to Kirchhoff's current law, the model of MNNs can be derived from the circuit implementation of MNNs shown in Figure 1. Therefore, the model of delayed MNNs is described as follows:

$$\begin{aligned}\mathcal{C}_k\frac{\mathrm{d}x_k(t)}{\mathrm{d}t} &= -[\sum_{l=1}^{n}(\mathcal{D}_{fkl}+\mathcal{H}_{fkl})+\frac{1}{\mathcal{R}_k}]+\sum_{l=1}^{n}\mathcal{D}_{fkl}f_l(x_l(t))\\ &\quad+\sum_{l=1}^{n}\mathcal{H}_{fkl}\mathrm{sgn}_{kl}f_l(x_l(t-\tau_l(t))+I_k(t),\end{aligned} \tag{1}$$

where $f_l(x_l(t-\tau_l(t)))$ and $f_l(x_l(t))$ are neural feedback functions used in the MNNs; $x_k(t)$ is the voltage of the capacitor $\mathcal{C}_k$; and $\mathcal{D}_{fkl}$ and $\mathcal{H}_{fkl}$ represent the memristance of the memristor $\mathbb{M}_{fkl}$ and $\mathbb{N}_{fkl}$, respectively. $\mathcal{R}_k$ denotes the resistance; $\tau_l(t)$ represents the transmission delay; and $0 \le \tau_l(t) \le \bar{\tau}_l$ and $\dot{\tau}_l(t) \le \tau_l < 1$. Here, τ_l is a constant, and it has a positive value. sgn_{kl} is a two-valued function determined by k and l; that is, $\mathrm{sgn}_{kl} = 1$ for $k \ge l$ and $\mathrm{sgn}_{kl} = -1$ for $k = l$.

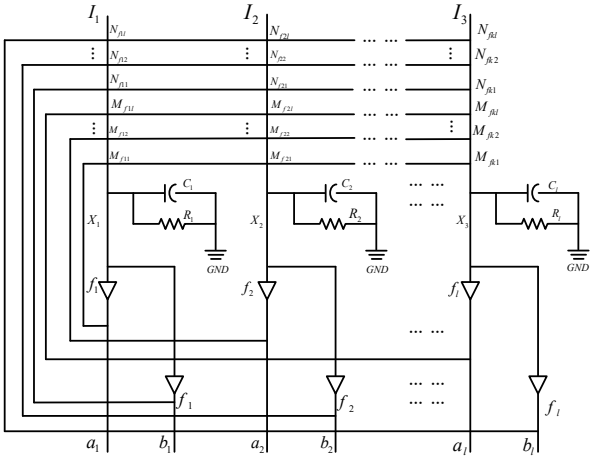

Figure 1. Circuit implementation of delayed MNNs.

To simplify the mathematical model of the memristor on the premise of obtaining the pinched hysteresis feature as shown in Figure 2, we select a surrogate model of MNNs defined by the following equation:

$$\frac{\mathrm{d}x_k(t)}{\mathrm{d}t} = -d_k(x_k(t))x_k(t)+\sum_{l=1}^{n}a_{kl}(x_k(t))f_l(x_l(t))+\sum_{l=1}^{n}b_{kl}(x_k(t-\tau_l(t)))f_l(x_l(t-\tau_l(t)))+I_k(t), \tag{2}$$

where $d_k(x_k(t))$ represents the self-inhibition of the k-th neuron in the MNNs; $a_{kl}(x_k(t))$ indicates the memristor's synaptic connection weight; and $b_{kl}(x_k(t-\tau_l(t)))$ is the memristor-based weight. Then, $d_k(x_k(t)) = \frac{1}{\mathcal{C}_k}[\sum_{l=1}^{n}(\mathbb{M}_{fkl} \text{ and } \mathbb{N}_{fkl})+\frac{1}{\mathcal{R}_k}]$, $a_{kl}(x_k(t)) = \frac{\mathbb{M}_{fkl}}{\mathcal{C}_k}\times\mathrm{sgn}_{kl}$, $b_{kl}(x_k(t-\tau_l(t)) = \frac{\mathbb{N}_{fkl}}{\mathcal{C}_k}\times\mathrm{sgn}_{kl}$.

Assume that $x(t) = (x_1(t), x_2(t), \ldots, x_k(t))^{\mathrm{T}}$ is a solution to MNNs (2) in the initial conditions of $x(s) = \phi(s) = (\phi_1(t), \phi_2(t), \ldots, \phi_k(t))^{\mathrm{T}} \in \mathcal{C}([-\tau_l, 0], \mathbb{R}^{\mathrm{T}})$. In particular, the solution can be further extended to $[0, +\infty]$ in Filippov's sense, and MNNs (2) could be taken to be the differential inclusion in this case. A category of MNNs having time-varying uncertainties, i.e., $\Delta a_{kl}(t)$ and $\Delta b_{kl}(t-\tau_l(t))$, is acquired in Equation (3).

$$\begin{aligned}\frac{\mathrm{d}x_k(t)}{\mathrm{d}t} &\in -co[d_k(x_k(t))]x_k(t)+\sum_{l=1}^{n}\Big[co[a_{kl}(x_k(t))]+\Delta a_{kl}(t)\Big]f_l(x_l(t))\\ &\quad+\sum_{l=1}^{n}\Big[co[b_{kl}(x_k(t-\tau_l(t)))]+\Delta b_{kl}(t-\tau_l(t)))\Big]f_l(x_l(t-\tau_l(t)))+I_k(t),\end{aligned} \tag{3}$$

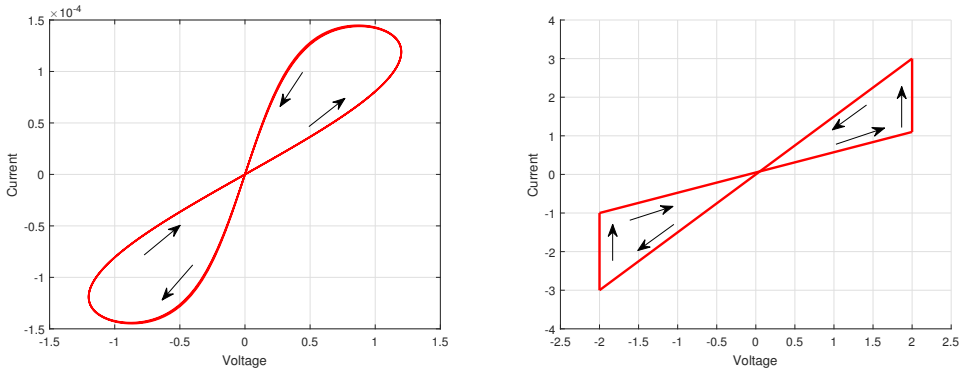

(**a**) (**b**)

Figure 2. The current and voltage characteristic of the memristor. (**a**) With a sinusoidal current. (**b**) The surrogate memristor model

According to the characteristics of a memristor, the state parameters in Equation (3) satisfy the following conditions:

$$co[d_k(x_k(t))] = \begin{cases} \acute{d_k}, & |x_k(t)| < \kappa_k, \\ co\{\acute{d}, \grave{d}\}, & |x_k(t)| = \kappa_k, \\ \grave{d_k}, & |x_k(t)| > \kappa_k, \end{cases} \quad co[a_{kl}(x_k(t))] = \begin{cases} \acute{a_{kl}}, & |x_k(t)| < \kappa_k, \\ co\{\acute{a_{kl}}, \grave{a_{kl}}\}, & |x_k(t)| = \kappa_k, \\ \grave{a_{kl}}, & |x_k(t)| > \kappa_k, \end{cases}$$

$$co[b_k(x_k(t-\tau_l(t)))] = \begin{cases} \acute{b_{kl}}, & |x_k(t-\tau_l(t))| < \kappa_k, \\ co\{\acute{b_{kl}}, \grave{b_{kl}}\}, & |x_k(t-\tau_l(t))| = \kappa_k, \\ \grave{b_{kl}}, & |x_k(t-\tau_l(t))| > \kappa_k. \end{cases} \tag{4}$$

According to the differential inclusion theory and set-valued map theory, Equation (3) could be considered a drive system. Considering the state-dependent and measurable functions $d_k^*(t) \in co[d_k(x_k(t))]$, $a_{kl}^*(t) \in co[a_{kl}(x_k(t))]$, $b_{kl}^*(t-\tau_l(t)) \in co[b_{kl}(x_k(t-\tau_l(t)))]$, we obtain

$$\begin{aligned} \frac{\mathrm{d}x_k(t)}{\mathrm{d}t} &= -d_k^*(t)x_k(t) + \sum_{l=1}^{n}\Big[a_{kl}^*(t) + \Delta a_{kl}(t)\Big]f_l(x_l(t)) \\ &\quad + \sum_{l=1}^{n}\Big[b_{kl}^*(t-\tau_l(t)) + \Delta b_{kl}(t-\tau_l(t)))\Big]f_l(x_l(t-\tau_l(t))) + I_k(t). \end{aligned} \tag{5}$$

Other parameters are defined in a similar way, and the introduction of the response system is shown in Equation (6).

$$\begin{aligned} \frac{\mathrm{d}y_k(t)}{\mathrm{d}t} &= -d_k^{**}(t)y_k(t) + \sum_{l=1}^{n}\Big[a_{kl}^{**}(t) + \overline{\Delta}a_{kl}(t)\Big]f_l(y_l(t)) \\ &\quad + \sum_{l=1}^{n}\Big[b_{kl}^{**}(t-\tau_l(t)) + \overline{\Delta}b_{kl}(t-\tau_l(t)))\Big]f_l(y_l(t-\tau_l(t))) + I_k(t) + U_k(t), \end{aligned} \tag{6}$$

where $y_k(t)$ indicates a state variable of the $k-th$ neuron in the MNNs ($k, l = 1, 2, \ldots, n$), and t is not less than zero.

Suppose that in the initial conditions of $y(s) = \varphi(s) = (\varphi_1(t), \varphi_2(t), \ldots, \varphi_k(t))^{\mathrm{T}} \in \mathcal{C}([-\tau_l, 0], \mathbb{R}^{\mathrm{T}})$, the solution to MNNs (6) is $y(t) = (y_1(t), y_2(t), \ldots, y_k(t))^{\mathrm{T}}$. In particular, $U_k(t)$ is a controller that can achieve exponential synchronization of the MNNs shown in Equations (5) and (6).

In Equations (5) and (6), $\Delta a_{kl}(t)$, $\Delta b_{kl}(t-\tau(t))$, $\overline{\Delta} a_{kl}(t)$, and $\overline{\Delta} b_{kl}(t-\tau(t))$ indicate time-varying uncertainties. Then, we have $|\Delta a_{kl}(\cdot)| \le a_{kl}$, $|\Delta b_{kl}(\cdot)| \le b_{kl}$, $|\overline{\Delta} a_{kl}(\cdot)| \le \overline{a}_{kl}$, and $\overline{\Delta} b_{kl}(\cdot)| \le \overline{b}_{kl}$. Consider N coupled MNNs (5) as follows

$$\begin{aligned} \frac{\mathrm{d}x_i(t)}{\mathrm{d}t} &= -D^*(t)x_i(t) + \Big[A^*(t) + \Delta A(t)\Big] f(x_i(t)) + \sigma \sum_{j=1}^{N} w_{ij}\Gamma x_j(t) \\ &\quad + \Big[B^*(t) + \Delta B(t)\Big] f(x_i(t-\tau(t))) + I_i(t),\ i = 1, 2, \ldots, N. \end{aligned} \tag{7}$$

Then, the CMNNs could be a drive system containing N identical MNNs, and it can be described as Equation (7). In this expression, $x_i(t) = (x_{i1}(t), x_{i2}(t), \ldots, x_{in}(t))^{\mathrm{T}} \in \mathbb{R}^n$ are the state variables of dynamical node i; the $D^*(t) = \mathrm{diag}(d_1^*(t), d_2^*(t), \ldots, d_N^*(t))^{\mathrm{T}}$, $A^*(t) = (a_{kl}^*(t))_{n\times n}$, $B^*(t) = (b_{kl}^*(t))_{n\times n}$, $\Delta A(t) = (\Delta a_{kl}(t))_{n\times n}$, $\Delta B(t-\tau(t)) = (\Delta b_{kl}(t-\tau(t)))_{n\times n}$; the constant $\sigma > 0$ refers to the coupling strength; the matrix $\Gamma = (r_{ij}) \in \mathbb{R}^{n\times n}$ is a nondelayed inner connecting matrix; and the coupled matrix $W = (w_{ij})_{N\times N}$ represents the whole network's topology, and it satisfies the following conditions: (H_1): diffusive coupling conditions are satisfied, i.e., $w_{ii} = -\sum_{j=1, j\neq i}^{N} w_{ij}$ for $i = 1, 2, \ldots, N$; (H_2): for a directed edge that points from node j to node i, $w_{ij} = 1$; otherwise, $w_{ij} = 0$.

Remark 1. *In recent scientific developments, MNNs have been widely applied in various fields, including knowledge acquisition, static image processing, secure communication, associative memory, motion tracking, and so on. These uncertainties refer to the unpredictable variations in the environmental conditions that affect signal transmission. These variations can be thought of as random fluctuations or disturbances that impact the accuracy of the synchronization made by the proposed method. Many problems in practice can be modeled using MNNs with random uncertainties. However, the mathematical formulation of these problems is difficult and needs more data-driven knowledge to clarify uncertainty bounds [23,24], which we will study in the near future.*

Then, the response system is shown in Equation (8):

$$\begin{cases} \dfrac{\mathrm{d}y_i(t)}{\mathrm{d}t} = -D^{**}(t)y_i(t) + \Big[A^{**}(t) + \overline{\Delta} A(t)\Big] f(y_i(t)) + \Big[B^{**}(t-\tau(t)) + \overline{\Delta} B(t-\tau(t))\Big] f(y_i(t-\tau(t))) \\ \qquad\qquad + \sigma \displaystyle\sum_{j=1}^{N} w_{ij}\Gamma y_j(t) + I_i(t) + U_i(t),\ i = 1, 2, \ldots, p, \\ \dfrac{\mathrm{d}y_i(t)}{\mathrm{d}t} = -D^{**}(t)y_i(t) + \Big[A^{**}(t) + \overline{\Delta} A(t)\Big] f(y_i(t)) + \Big[B^{**}(t-\tau(t)) + \overline{\Delta} B(t-\tau(t))\Big] f(y_i(t-\tau(t))) \\ \qquad\qquad + \sigma \displaystyle\sum_{j=1}^{N} w_{ij}\Gamma y_j(t) + I_i(t),\ i = p+1, p+2, \ldots, N, \end{cases} \tag{8}$$

where $U_i(t)$, $i = 1, 2, \ldots, p$ represents a nonlinear pinning controller. In Equation (8), $y_i(t) = (y_{i1}(t), y_{i2}(t), \ldots, y_{in}(t))^{\mathrm{T}} \in \mathbb{R}^n$ are scalars corresponding to the response state. Here, make the first p nodes in control and rearrange the nodes' order in the networks. Additionally, $D^{**}(t) = \mathrm{diag}(d_1^{**}(t), d_2^{**}(t), \ldots, d_N^{**}(t))^{\mathrm{T}}$, $A^{**}(t) = (a_{kl}^{**}(t))_{n\times n}$, $B^{**}(t-\tau(t)) = (b_{kl}^{**}(t-\tau(t)))_{n\times n}$, $\overline{\Delta} A(t) = (\overline{\Delta} a_{kl}(t))_{n\times n}$, $\overline{\Delta} B(t-\tau(t)) = (\overline{\Delta} b_{kl}(t-\tau(t)))_{n\times n}$.

2.2. Error Systems of CMNNs

The synchronization error is formulated as $\epsilon_i(t) = \big((y_{i1}(t) - x_{i1}(t)), (y_{i2}(t) - x_{i2}(t)), \ldots, (y_{in}(t) - x_{in}(t))\big)^{\mathrm{T}} \in (\epsilon_{i1}(t), \epsilon_{i2}(t), \ldots, \epsilon_{in}(t))^{\mathrm{T}}$ with the initial condition $\epsilon(s) = \varphi(s) - \phi(s) = \psi(s) \in \mathcal{C}([-\tau_l, 0], \mathbb{R}^{\mathrm{T}})$. The design of the nonlinear hybrid controller $U_i(t)$ is:

$$\begin{cases} U_i(t) = K_i\epsilon_i(t_{k-1}) + \displaystyle\sum_{k=1}^{\infty} [\mu_k\epsilon_i(t) - \epsilon_i(t)]\delta(t - t_{k-1}), \quad i = 1, 2, \ldots, p, \\ U_i(t) = 0, \quad i = p+1, p+2, \ldots, N, \end{cases} \tag{9}$$

where $t \in [t_{k-1}, t_k), k \in N, \mu_k \geq 0$,$t_k$ represents the impulsive time instants that conform to $0 = t_0 < t_1 < t_2 < \ldots < t_{k-1} < t_k < \ldots$; $\lim_{k\to+\infty} t_k = +\infty$; $K_i \in R$ represents the gain of state feedback control; and $\delta(\cdot)$ refers to the Dirac impulsive function, and its definition is shown below

$$\delta(t - t_k) = \begin{cases} +\infty, & t = t_k, k \in N, \\ 0, & t \geq t_k. \end{cases} \tag{10}$$

Here, $t_0 = 0$ is the initial time, and $\{t_1, t_2, t_3, \ldots\}$ represents time instants that are determined by a series of subsequence events. It is assumed $\epsilon(t)$ shows right continuity at the time $t = t_k$, i.e., $\epsilon_i(t_k) = \epsilon_i(t_{k+1})$. Thus, the solution to the error system exhibits jumping discontinuity under impulse at $t = t_k$. In particular, the state information in Equation (8) is considered a control input and sent to Equation (7). This will cause the state variables in the error system to change immediately at $t = t_k$.

Remark 2. *The pinning event-triggered scheme (PETS) for the proposed CMNNs is demonstrated in Figure 3. It can be seen that only the local information has been utilized by the PETS, which differs from some existing results in [25,26]. Moreover, "pinning" does not mean the fractional of nodes is controlled but implies that such local information of the pinned nodes is taken advantage of by the triggered instants t_k determined. Then, the information $\epsilon_i(t_k)$ can be exchanged from CMNNs to actuators at each instant t_k. Meanwhile, the sample has arisen in event generators and the PETS is activated for the whole system until the new loop relays on the updated event.*

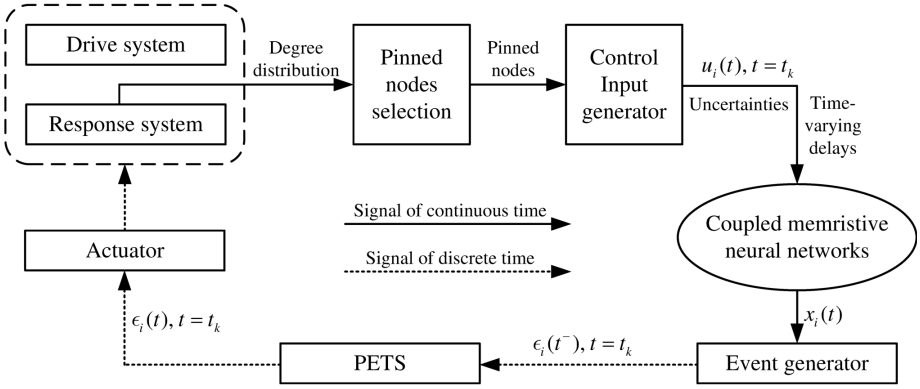

Figure 3. A block diagram of PETS.

Based on this, the event-triggered impulsive hybrid controller error system with state feedback can be designed as

$$\begin{cases} \dfrac{\mathrm{d}\epsilon_i(t)}{\mathrm{d}t} = -\big(D^{**}(t)y_i(t) - D^{*}(t)x_i(t)\big) + F_A(t) + F_{\Delta A}(t) + F_B(t-\tau(t)) + F_{\Delta B}(t-\tau(t)) \\ \qquad + \sigma\sum_{j=1}^{N} w_{ij}\Gamma\epsilon_j(t) + K_i\epsilon_i(t_{k-1}), t \in [t_{k-1},\ t_k), k \in N, i = 1, 2, \ldots, p, \\ \dfrac{\mathrm{d}\epsilon_i(t_k^+)}{\mathrm{d}t} = \mu_k\epsilon_i(t_k^-), \mu_k \neq 0,\ t = t_k, i = 1, 2, .., p, \\ \dfrac{\mathrm{d}\epsilon_i(t)}{\mathrm{d}t} = -\big(D^{**}(t)y_i(t) - D^{*}(t)x_i(t)\big) + F_A(t) + F_{\Delta A}(t) + F_B(t-\tau(t)) + F_{\Delta B}(t-\tau(t)) \\ \qquad + \sigma\sum_{j=1}^{N} w_{ij}\Gamma\epsilon_j(t),\ i = p+1, p+2, \ldots, N, \end{cases} \tag{11}$$

where $F_A(t) = A^{**}(t)f(y_i(t)) - A^{*}(t)f(x_i(t))$, $F_{\Delta A}(t) = \overline{\Delta}A(t)f(y_i(t)) - \Delta A(t)f(x_i(t))$, $F_B(t-\tau(t)) = B^{**}(t-\tau(t))f(y_i(t-\tau(t))) - B^{*}(t-\tau(t))f(x_i(t-\tau(t)))$, $F_{\Delta B}(t-\tau(t)) = \overline{\Delta}B(t-\tau(t))f(y_i(t-\tau(t))) - \Delta B(t-\tau(t))f(y_i(t-\tau(t)))$. $K_i\epsilon_i(t_{k-1})$ is the control input with state feedback. In addition, the impulsive control can only work at time t_k.

Then, for $i = 1, 2, \ldots, N$, the measurement error of Equation (11) is:

$$e_i(t) = \epsilon_i(t_{k-1}) - \epsilon_i(t), t \in [t_{k-1}, t_k), k \in N. \tag{12}$$

and $e(t)$ satisfies $e(t) = (e_1(t), e_2(t), \ldots, e_N(t))^{\mathrm{T}}$.

2.3. Some Useful Definitions and Assumptions

Before investigating the exponential synchronization of Systems (7) and (8), some related assumptions, definitions, and lemmas are given.

Assumption 1 ([27]). *The activation function $f_i(\cdot)$ is Lipschitz continuous. In this case, positive scalars L_f exist such that*

$$|f_j(\kappa_1) - f_j(\kappa_2)| \leq L_f|\kappa_1 - \kappa_2|, \tag{13}$$

for all $\kappa_1 \in \mathbb{R}$, $i \in N$.

Assumption 2 ([28]). *For any $i \in N$, $f_i(\cdot)$ is a bounded activation function, i.e., it satisfies the positive constant $M_i > 0$:*

$$|f_i(s)| \leq M_i, \forall s \in \mathbb{R}. \tag{14}$$

Assumption 3 ([29]). *The matrix W is irreducible if matrix Γ is positive definite, which means that there is no isolated node.*

Lemma 1 ([30]). *Supposing that real matrices X and Y have appropriate dimensions, a positive number α exists such that*

$$X^T Y + Y^T X \leq \alpha X^T X + \alpha^{-1} Y^T Y \tag{15}$$

Lemma 2 ([27]). *Let*

$$0 \leq \tau_i(t) \leq \bar{\tau}, F(t, u, \bar{u}_1, \ldots, \bar{u}_m) : R^+ \times \underbrace{R \times R}_{m+1} \to R \tag{16}$$

and do not decrease in $\bar{u}_i$ for a fixed $(t, u, \bar{u}_1, \ldots, \bar{u}_m)$, where $i = 1, 2, \ldots, m$. Additionally, let $I_k(u) : R \to R$ and do not decrease in u. Assume that u_t, $v(t)$ satisfy

$$\begin{cases} D^+u(t) \leq F(t, u(t), u(t - \tau_1(t)), \ldots, u(t - \tau_m(t))), t \geq 0, \\ u(t_k) \leq I_k(u(t^-)k)), k \in N_+, \end{cases} \tag{17}$$

and

$$\begin{cases} D^+u(t) > F(t, v(t), v(t - \tau_1(t)), \ldots, v(t - \tau_m(t))), t \geq 0, \\ v(t_k) \leq I_k(v(t^-)k)), k \in N_+, \end{cases} \tag{18}$$

where $D^+y(t)$ represents the upper right Dini derivative, and $D^+y(t) = \overline{\lim_{h \to 0^+}} \frac{y(t+h)-y(t)}{h}$; and $h \to 0^+$ indicates that h is approximated to 0 from the right-hand side. For $-\overline{\tau} \leq t \leq 0$, $u(t) \leq v(t)$ indicates that $u(t) \leq v(t)$ $(t \geq 0)$.

Lemma 3 ([29]). *It is supposed that the continuous function $V(t)$ corresponds to a nonnegative value if $t \in (a - \overline{\tau}, +\infty)$ conforms to the following:*

$$\dot{V}(t) \leq -k_1 V(t) + k_2 \max_{t - \overline{\tau} \leq s \leq a} V(s) exp\{-r(t - a)\}, t \geq a. \tag{19}$$

and r is a unique and positive solution to

$$r - k_1 + k_2 exp\{r\overline{\tau}\} = 0. \tag{20}$$

Lemma 4 ([31]). *Based on Assumptions 1 and 2, the following expression is formulated*

$$\begin{aligned}
&|d_k^{**} y_k(t) - d_k^{*} x_k(t)| \le d_k^{+} |y_k(t) - x_k(t)|,\\
&|a_{kl}^{**} f(y_k(t)) - a_{kl}^{*} f(x_k(t))| \le a_{kl}^{+} L_f |y_k(t) - x_k(t)|,\\
&|b_{kl}^{**} f(y_k(t-\tau(t))) - b_{kl}^{*} f(x_k(t-\tau(t))| \le b_{kl}^{+} L_f |y_k(t-\tau(t)) - x_k(t-\tau(t))|,\\
&|\overline{\Delta} a_{kl} f(y_k(t)) - \Delta a_{kl} f(x_k(t))| \le \tilde{a}_{kl}^{+} L_f |y_k(t) - x_k(t)|,\\
&|\overline{\Delta} b_{kl} f(y_k(t-\tau(t))) - \Delta b_{kl} f(x_k(t-\tau(t)))| \le \tilde{b}_{kl}^{+} L_f |y_k(t-\tau(t)) - x_k(t-\tau(t))|,
\end{aligned} \tag{21}$$

where $D = diag\{d_1^+, d_2^+, \ldots, d_N^+\}$, $A^+ = L_f(a_{kl}^+)_{n\times n}$, $B^+ = L_f(b_{kl}^+)_{n\times n}$, $\tilde{A}^+ = L_f(\tilde{a}_{kl}^+)_{n\times n}$, $\tilde{B}^+ = L_f(\tilde{b}_{kl}^+)_{n\times n}$, $d_k^+ = max\{|\acute{d}_k|, |\grave{d}_k|\}$, $a_{kl}^+ = max\{|\acute{a}_{kl}|, |\grave{a}_{kl}|\}$, $b_{kl}^+ = max\{|\acute{b}_{kl}|, |\grave{b}_{kl}|\}$, $\tilde{a}_{kl}^+ = max\{|a_{kl}|, |\overline{a}_{kl}|\}$, $\tilde{b}_{kl}^+ = max\{|b_{kl}|, |\overline{b}_{kl}|\}$.

Definition 1 ([28]). *The drive system, Equation (7), and the response system, Equation (8), are said to be exponentially synchronized according to the control strategy, Equation (43). Constants* $\mu > 0$, $M \ge 1$ *exist such that for* $t \ge 0$,

$$||e(t)|| \le Mexp\{-\mu t\} \max_{t-\overline{\tau}\le s\le 0} ||\psi(s)||, \tag{22}$$

then, $e(t) = (e_1^T(t), e_2^T(t), \ldots, e_N^T(t))^T$, $\psi(s) = (\psi_1^T(s), \psi_2^T(s), \ldots, \psi_N^T(s))^T$.

Definition 2 ([32]). *The error system (11) does not have Zeno behaviors if constant* $\rho > 0$ *exists such that*

$$\inf_{k\in N_+} \{t_k - t_{k-1}\} \ge \rho > 0. \tag{23}$$

Remark 3. *Zeno behavior is the phenomenon where events are triggered an infinite number of times within a finite time. The event-triggered strategy with Zeno behavior is equivalent to continuous communication. If Zeno behavior is not excluded, the event-triggered strategy is ineffective. This not only fails to reduce the utilization of communication resources but also adversely affects the stability of the system.*

3. Main Results

3.1. Synchronization of CMNNs

This section presents the solution to the exponential synchronization of delayed uncertain CMNNs under the proposed PETS strategy.

To present results, this paper gives the denotations as follows, $\bar{R} = \text{diag}\{\underbrace{r, r, r}_{p}, \underbrace{\ldots, 0, 0, 0}_{N-p}\}$, $\hat{w}_{ij} = w_{ij} (i \ne j)$, $\tilde{\lambda} = \lambda_{\max}(\hat{W}^s - \bar{R})$, $\hat{W} = (\hat{w}_{ij})_{N\times N}$, $\hat{w}_{ii} = \frac{\lambda_{\min}(\Gamma^s)}{||\Gamma||}$, $||W|| = (\lambda_{\max}(W^{\mathrm{T}}W))^{\frac{1}{2}}$, $W^s = \frac{1}{2}(W + W^{\mathrm{T}})$.

Theorem 1. *Based on Assumptions 1 and 2, Systems (7) and (8) demonstrate pinning exponential synchronization with the control law (9) if there exist constants* $\rho_2 \ge \rho_1 > 0$, $\varepsilon_q > 0$ $(q = 1, 2, 3)$, *such that*

$$\mu_k^2 \ge 1, \tag{24}$$

$$-\left(\frac{ln\tilde{\mu}}{\rho_1} + \varpi_1\right) > \tilde{\mu}\beta_1 > 0, \tag{25}$$

$$\Lambda = \varpi_2 + \beta_1 < 0, \tag{26}$$

$$\tilde{\alpha} - (\frac{1}{2}\varepsilon_1^{-1})\lambda_{max}||B^+||^2 + (\frac{1}{2}\varepsilon_2^{-1})\lambda_{max}||\tilde{B}^+||^2 - \frac{1}{2}\varepsilon_3 K_i^2 > 0,\ i = 1, 2, ..., p, \tag{27}$$

$$\eta(t) < 0, \quad t \in [t_{k-1}, t_k), \tag{28}$$

where $k \in N_+$, $\varpi_1 = -\lambda_{min}(D^+) + \lambda_{max}(A^+) + \lambda_{max}(\tilde{A}^+) + K_i + \tilde{\alpha} + \sigma(r + \tilde{\lambda})||\Gamma||$, $\beta = \beta_1 = \beta_2 = \frac{1}{2}(\varepsilon_1 + \varepsilon_2)$, $\tilde{\mu} = \max_k\{\mu_k^2\}$, $\mu_k \neq 0$, $\varpi_2 = -\lambda_{min}(D^+) + \lambda_{max}(A^+) + \lambda_{max}(\tilde{A}^+) + \frac{1}{2}\varepsilon_1^{-1}\lambda_{max}(||B^+||^2) + \frac{1}{2}\varepsilon_2^{-1}\lambda_{max}(||\tilde{B}^+||^2) + \sigma\tilde{\lambda}||\Gamma||$.

This paper designs the triggered function as

$$\eta_i(t) = ||e_i(t)||^2 - \varepsilon_3|\epsilon_i(t)|\big[\tilde{\alpha} - \frac{1}{2}\varepsilon_1^{-1}\lambda_{\max}(||B^+||^2) + \frac{1}{2}\varepsilon_2^{-1}\lambda_{\max}(||\tilde{B}^+||^2) - \frac{1}{2}\varepsilon_3 K_i^2\big]|\epsilon_i(t)|. \tag{29}$$

The triggered instant t_k depends on the event-triggered condition shown in Equation (30)

$$t_k = \inf_t\{t \in (t_{k-1}, \infty)|\eta(t) \geq 0\}. \tag{30}$$

Systems (7) and (8) can achieve pinning exponential synchronization.

In addition, if Equations (26)–(28) and (30) hold, Equations (24) and (2) can be rewritten as the following inequalities

$$0 < \mu_k^2 < 1, \tag{31}$$

$$-\Big(\frac{\ln\tilde{\mu}}{\rho_2} + \varpi_1\Big) > \tilde{\mu}^{-1}\beta_1 > 0. \tag{32}$$

Proof. For System (11), consider the nonnegative function as

$$V(t) = \frac{1}{2}\sum_{i=1}^{N}\epsilon_i^{\mathrm{T}}(t)\epsilon_i(t). \tag{33}$$

Let

$$V_1(t) = \sum_{i=1}^{p}\epsilon_i^{\mathrm{T}}(t)\epsilon_i(t), \qquad V_2(t) = \sum_{i=p+1}^{N}\epsilon_i^{\mathrm{T}}(t)\epsilon_i(t). \tag{34}$$

When $V(t)$ and the solution to (11) are differentiated for the $[t_{k-1}, t_k)$,$k \in N_+$, there is

$$D^+V(t) = \sum_{i=1}^{N}\epsilon_i^{\mathrm{T}}(t)\dot{\epsilon}_i(t) + \sum_{i=1}^{p}\epsilon_i^{\mathrm{T}}(t)U_i(t). \tag{35}$$

Let $D^+V_a(t) = \sum_{i=1}^{N}\epsilon_i^{\mathrm{T}}(t)\dot{\epsilon}_i(t)$ and $D^+V_b(t) = \sum_{i=1}^{p}\epsilon_i^{\mathrm{T}}(t)U_i(t)$. For $\dot{V}_a(t)$, we have

$$\begin{aligned} D^+V_a(t) &= \sum_{i=1}^{N}\epsilon_i^{\mathrm{T}}(t)\Big[-\big(D^{**}(t)y_i(t) - D^*(t)x_i(t)\big) + F_A(t) + F_{\Delta A}(t) + F_B(t-\tau(t)) \\ &\quad + F_{\Delta B}(t-\tau(t)) + \sigma\sum_{j=1}^{N}w_{ij}\Gamma\epsilon_j(t)\Big] \\ &\leq \sum_{i=1}^{N}\Big[-\epsilon_i^{\mathrm{T}}(t)|D^{**}(t)y_i(t) - D^*(t)x_i(t)| + \epsilon_i^{\mathrm{T}}(t)|F_A(t)| + \epsilon_i^{T}(t)|F_B(t-\tau(t))| \\ &\quad + \epsilon_i^{\mathrm{T}}(t)|F_{\Delta A}(t)| + \epsilon_i^{T}(t)|F_{\Delta B}(t-\tau(t))| + \epsilon_i^{\mathrm{T}}(t)\sigma\sum_{j=1}^{N}w_{ij}\Gamma\epsilon_j(t)\Big]. \end{aligned} \tag{36}$$

Combining with Lemma 1 and Lemma 4, we have

$$\begin{aligned}
&-\epsilon_i^{\mathrm{T}}(t)|D^{**}(t)y_i(t) - D^{*}(t)x_i(t)| \le -\epsilon_i^{\mathrm{T}}(t)\lambda_{\min}(D^{+})\epsilon_i(t),\\
&\epsilon_i^{\mathrm{T}}(t)|F_A(t)| \le \epsilon_i^{\mathrm{T}}(t)\lambda_{\max}(A^{+})\epsilon_i(t),\\
&\epsilon_i^{\mathrm{T}}(t)|F_{\Delta A}(t)| \le \epsilon_i^{\mathrm{T}}(t)\lambda_{\max}(\tilde{A}^{+})\epsilon_i(t),\\
&\epsilon_i^{\mathrm{T}}(t)|F_B(t-\tau(t))| \le \epsilon_i^{\mathrm{T}}(t)\lambda_{\max}(B^{+})\epsilon_i(t-\tau(t)),\\
&\epsilon_i^{\mathrm{T}}(t)|F_{\Delta B}(t-\tau(t))| \le \epsilon_i^{\mathrm{T}}(t)\lambda_{\max}(\tilde{B}^{+})\epsilon_i(t-\tau(t)).
\end{aligned} \tag{37}$$

Then, there is

$$\begin{aligned}
\epsilon_i^{\mathrm{T}}(t)\lambda_{\max}(B^{+})\epsilon_i(t-\tau(t)) &\le \frac{1}{2}\varepsilon_1^{-1}\epsilon_i^{\mathrm{T}}(t)\lambda_{\max}(B^{+})\lambda_{\max}(B^{+})^{\mathrm{T}}\epsilon_i(t) + \frac{1}{2}\varepsilon_1\epsilon_i^{\mathrm{T}}(t-\tau(t))\epsilon_i(t-\tau(t))\\
&\le \frac{1}{2}\varepsilon_2^{-1}||\lambda_{\max}(\tilde{B}^{+})||^2\epsilon_i^{\mathrm{T}}(t)\epsilon_i(t) + \frac{1}{2}\varepsilon_2\epsilon_i^{\mathrm{T}}(t-\tau(t))\epsilon_i(t-\tau(t)).
\end{aligned} \tag{38}$$

Considering that $w_{ii} < 0$, $i = 1, 2, \ldots, N$, in this condition, we have the inequality shown in Equation (39)

$$\begin{aligned}
\epsilon_i^{\mathrm{T}}(t)\sigma\sum_{j=1}^{N} w_{ij}\Gamma\epsilon_j(t) &\le \sigma||\Gamma||\sum_{i=1}^{N}\sum_{j=1,j\neq i}^{N} w_{ij}||\epsilon_i^{\mathrm{T}}(t)||_2||\epsilon_j(t)||_2 + \sigma\lambda_{\min}(\Gamma^s)\sum_{i=1}^{N} w_{ii}\epsilon_i^{\mathrm{T}}(t)\epsilon_i(t)\\
&= \sigma||\Gamma||\tilde{\epsilon}^{\mathrm{T}}(t)\hat{W}^s\tilde{\epsilon}(t)\\
&= \sigma\sum_{i=1}^{p}(r+\tilde{\lambda})||\Gamma||\epsilon_i^{\mathrm{T}}(t)\epsilon_i(t) + \sigma\sum_{i=p+1}^{N}||\Gamma||\tilde{\lambda}\epsilon_i^{\mathrm{T}}(t)\epsilon_i(t)
\end{aligned} \tag{39}$$

In Equation (39), $\tilde{\epsilon}(t) = \left(||\epsilon_1(t)||_2, ||\epsilon_2(t)||_2, \ldots, ||\epsilon_N(t)||_2\right)^{\mathrm{T}}$. According to Assumption 3, W is irreducible, so $\hat{W}^s$ is also irreducible. According to the discussion in [29], $\tilde{\lambda} = \lambda_{\max}(\hat{W}^s - \tilde{R}) < 0$ holds for any positive constant.

Then, there is

$$\begin{aligned}
D^{+}V_a(t) \le \sum_{i=1}^{N}\epsilon_i^{\mathrm{T}}(t)\Big[&\epsilon_i^{-\mathrm{T}}(t)\lambda_{\min}(D^{+})\epsilon_i(t) + \epsilon_i^{\mathrm{T}}(t)\lambda_{\max}(A^{+})\epsilon_i(t)\\
&+ \epsilon_i^{\mathrm{T}}(t)\lambda_{\max}(\tilde{A}^{+})\epsilon_i(t) + \frac{1}{2\varepsilon_1}\epsilon_i^{\mathrm{T}}(t)||\lambda_{\max}(B^{+})||^2\epsilon_i(t) + \frac{\varepsilon_1}{2}\epsilon_i^{\mathrm{T}}(t-\tau(t))\epsilon_i(t-\tau(t))\\
&+ \frac{1}{2\varepsilon_2}\epsilon_i^{\mathrm{T}}(t)||\lambda_{\max}(\tilde{B}^{+})||^2\epsilon_i(t) + \frac{\varepsilon_2}{2}\epsilon_i^{\mathrm{T}}(t-\tau(t))\epsilon_i(t-\tau(t))\Big]\\
&+ \sigma\sum_{i=1}^{p}(r+\tilde{\lambda})||\Gamma||\epsilon_i^{\mathrm{T}}(t)\epsilon_i(t) + \sigma\sum_{i=p+1}^{N}||\Gamma||\tilde{\lambda}\epsilon_i^{\mathrm{T}}(t)\epsilon_i(t).
\end{aligned} \tag{40}$$

For

$$D^{+}V_b(t) = \sum_{i=1}^{p}\epsilon_i^{\mathrm{T}}(t)U_i(t), \tag{41}$$

the measurement error introduced to Equation (11) is expressed as

$$e_i(t) = \epsilon_i(t_{k-1}) - \epsilon_i(t), \quad t \in [t_{k-1}, t_k), k \in N_+, i = 1, 2, \ldots, p. \tag{42}$$

Here, the controller (9) can be transformed into

$$U_i(t) = K_i\epsilon_i(t_{k-1}). \tag{43}$$

Next, the event-triggered function $\eta_i(t)$ shown in Equation (29) is designed, and it should satisfy $\eta_i(t) < 0, t \in [t_{k-1}, t_k)$.

After combining with the mentioned condition, consider $D^{+}V_b(t)$ such that

$$\begin{aligned} D^+V_b(t) &= \sum_{i=1}^{p} \epsilon_i^{\mathrm{T}}(t)K_i(\epsilon_i(t)+e_i(t)) \\ &\le \sum_{i=1}^{p} \epsilon_i^{\mathrm{T}}(t)K_i\epsilon_i(t) + \frac{\varepsilon_3}{2}\sum_{i=1}^{p} \epsilon_i^{\mathrm{T}}(t)K_i^2\epsilon_i(t) + \frac{1}{2\varepsilon_3}\sum_{i=1}^{p} e_i^{\mathrm{T}}(t)e_i(t) \\ &= \sum_{i=1}^{p} \Big[\epsilon_i^{\mathrm{T}}(t)\big(K_i + \frac{1}{2}K_i^2\big)\epsilon_i(t) + \frac{1}{2\varepsilon_3}e_i^{\mathrm{T}}(t)e_i(t)\Big] \end{aligned} \tag{44}$$

Combining with $D^+V_a(t)$ and $D^+V_b(t)$, there is

$$\begin{aligned} D^+V(t) \le &\sum_{i=1}^{N}\Big[-\lambda_{\min}(D^+) + \lambda_{\max}(A^+) + \lambda_{\max}(\tilde{A}^+) + \frac{1}{2\varepsilon_1}\lambda_{\max}(B^+)||^2 + \frac{1}{2\varepsilon_2}\lambda_{\max}(\tilde{B}^+)||^2\Big] \\ &+ \sum_{i=1}^{N}\frac{\varepsilon_1+\varepsilon_2}{2}\epsilon_i^{\mathrm{T}}(t-\tau(t))\epsilon_i(t-\tau(t)) + \sum_{i=1}^{p}\epsilon_i^{\mathrm{T}}(t)\big[K_i + \frac{\varepsilon_3}{2}K_i^2 + \sigma(r+\tilde{\lambda})||\Gamma||\big] \\ &+ \sum_{i=1}^{p}\frac{1}{2\varepsilon_3}e_i^{\mathrm{T}}(t)e_i(t) + \sigma\sum_{i=p+1}^{N}||\Gamma||\tilde{\lambda}\epsilon_i^{\mathrm{T}}(t)\epsilon_i(t) \end{aligned} \tag{45}$$

Taking $\eta_i(t) < 0$ into consideration, we have

$$\begin{aligned} D^+V(t) \le &\sum_{i=1}^{p}\epsilon_i^{\mathrm{T}}(t)\Big[-\lambda_{\min}(D^+) + \lambda_{\max}(A^+) + \lambda_{\max}(\tilde{A}^+) + K_i + \tilde{\alpha} + \sigma(r+\tilde{\lambda})||\Gamma||\Big]\epsilon_i(t) \\ &+ \sum_{i=p+1}^{N}\epsilon_i^{\mathrm{T}}(t)\Big[-\lambda_{\min}(D^+) + \lambda_{\max}(A^+) + \lambda_{\max}(\tilde{A}^+) \\ &+ \frac{1}{2\varepsilon_1}\lambda_{\max}(B^+)||^2 + \frac{1}{2\varepsilon_2}\lambda_{\max}(\tilde{B}^+)||^2 + \sigma||\Gamma||\tilde{\lambda}\Big]\epsilon_i(t) \\ &+ \sum_{i=1}^{p}\frac{\varepsilon_1+\varepsilon_2}{2}\epsilon_i^{\mathrm{T}}(t-\tau(t))\epsilon_i(t-\tau(t)) + \sum_{i=p+1}^{N}\frac{\varepsilon_1+\varepsilon_2}{2}\epsilon_i^{\mathrm{T}}(t-\tau(t))\epsilon_i(t-\tau(t)). \end{aligned} \tag{46}$$

According to Equation (34), we have

$$D^+V_1(t) \le \varpi_1(t) + \beta_1 V_1(t-\tau(t)). \tag{47}$$

$$D^+V_2(t) \le \varpi_2(t) + \beta_2 V_2(t-\tau(t)). \tag{48}$$

That is,

$$D^+V(t) \le \varpi_1(t) + \beta_1 V_1(t-\tau(t)) + \varpi_2(t) + \beta_2 V_2(t-\tau(t)), \tag{49}$$

for $t \in [t_{k-1}, t_k)$, $k \in N_+$.

Here, the stability of Equations (47) and (48) is discussed, respectively. When $t = t_k$, $i = 1, 2, \ldots, p$, $k \in N_+$, according to Equation (11), we have

$$V_1(t_k^+) = (\mu_k\epsilon(t_k^-))^{\mathrm{T}}(\mu_k\epsilon(t_k^-)) = \mu_k^2 V_1(t_k^-). \tag{50}$$

When $\delta > 0$, for the delayed impulsive system shown in Equation (51) and Lemma 2, suppose $v(t)$ is a unique solution:

$$\begin{cases} D^+v(t) = \varpi_1 v(t) + \beta_1 v(t-\tau(t)) + \delta, t \ne t_k, t \ge 0, \\ v(t_k^+) = \mu_k^2 v(t_k^-), k \in N_+, \\ v(t) = ||\epsilon(t)||^2, -\tau_l \le t \le 0. \end{cases} \tag{51}$$

With the variable parameter formula,

$$V_1(t) \leq v(t), t \geq 0. \tag{52}$$

The expression of $v(t)$ is written as

$$v(t) = W(t) + \int_0^t W(t)(\beta_1 v(s-\tau(s)) + \delta)\mathrm{d}s, t \geq 0. \tag{53}$$

In Equation (53), $W(t)$ means the Cauchy matrix for Equation (54)

$$\begin{cases} D^+ v(t) = \varpi_1 v(t), t \neq t_k, t \geq 0. \\ v(t_k^+) = \mu_k^2 v(t_k^-), k \in N_+. \end{cases} \tag{54}$$

We have $W(t) = \mathrm{e}^{\varpi_1(t-s)} \prod\limits_{s \leq t_k \leq t} \mu_k^2$.

Remark 4. *For the calculation of triggered constants t_k, taking the definition of the Lyapunov function $V(t)$ and the relationship between measurement error $e_i(t)$ and synchronization error $\epsilon_i(t)$ into account, triggered function $\eta_i(t)$ is designed as Equation (29) to convert Equation (45) to the form that Lemma 2 needs as shown in Equation (46). Notably, the triggered function is derived from Equation (41), which means the proposed triggered function contains more information about the pinning scheme for the event-triggered control method.*

Case 1: For $\mu_k^2 \geq 1$.

As will be proved in Theorem 1, $\inf\limits_{k \in N_+} \{t_k - t_{k-1}\} > 0$, and a constant ρ_1 exists and satisfies $\inf\limits_{k \in N_+} \{t_k - t_{k-1}\} \geq \rho_1 > 0$. Then,

$$W(t) \leq \mathrm{e}^{\varpi_1(t-s)} \tilde{\mu}^{(\frac{t-s}{\rho_1}+1)} \leq \tilde{\mu} \mathrm{e}^{(\frac{\ln \tilde{\mu}}{\rho_1}+\varpi_1)(t-s)}, \tag{55}$$

and $\tilde{\mu} = \max\limits_k \{\mu_k^2\}$.

Substituting Equation (55) into Equation (51) yields

$$v(t) \leq \tilde{\mu} \mathrm{e}^{(\frac{\ln \tilde{\mu}}{\rho_1}+\varpi_1)t} ||\epsilon(0)||^2 + \int_0^t \tilde{\mu} \mathrm{e}^{(\frac{\ln \tilde{\mu}}{\rho_1}+\varpi_1)(t-s)} \Big[\beta_1 v(s-\tau(s)) + \delta\Big] \mathrm{d}s, \tag{56}$$

that is,

$$v(t) \leq \zeta \mathrm{e}^{(\frac{\ln \tilde{\mu}}{\rho_1}+\varpi_1)t} + \int_0^t \mathrm{e}^{(\frac{\ln \tilde{\mu}}{\rho_1}+\varpi_1)(t-s)} \Big[\tilde{\mu}\beta_1 v(s-\tau(s)) + \tilde{\mu}\delta\Big] \mathrm{d}s, \tag{57}$$

where $\zeta = \tilde{\mu} \sup\limits_{\tau_l \leq t \leq 0} \{||\epsilon(t)||^2\}$.

Let $\hbar(\rho) = 2\rho + \frac{\ln \tilde{\mu}}{\rho_1} + \varpi_1 + \tilde{\mu}\beta_1 \mathrm{e}^{2\rho\tau_l}$. For the continuous function $\hbar(\rho)$, according to (2), $\hbar(0) < 0$, $\hbar(+\infty) > 0$, and $\dot{\hbar}(\rho) = 2 + 2\tau_l \tilde{\mu}\beta_1 \mathrm{e}^{2\rho\tau_l} > 0$. Moreover, a unique solution $\rho > 0$ to $\dot{\hbar}(\rho) = 0$ exists.

For $-\tau_l \leq t \leq 0$, $\rho > 0$ and $\delta > 0$ hold, and we have $r > 0$ and $\tilde{\mu} \leq 1$. Thus,

$$\zeta \mathrm{e}^{(\frac{\ln \tilde{\mu}}{\rho_1}+\varpi_1)t} \leq \tilde{\mu} ||\epsilon(t)||^2 \mathrm{e}^{(\frac{\ln \tilde{\mu}}{\rho_1}+\varpi_1)t} \leq \tilde{\mu} ||\epsilon(t)||^2 \mathrm{e}^{-2\rho t} = \zeta \mathrm{e}^{-2\rho t}, \tag{58}$$

and

$$\begin{aligned} \int_0^t \mathrm{e}^{(\frac{\ln \tilde{\mu}}{\rho_1}+\varpi_1)(t-s)} \Big[\tilde{\mu}\beta_1 v(s-\tau(s)) + \tilde{\mu}\delta\Big] \mathrm{d}s &\leq \int_0^t \mathrm{e}^{(\frac{\ln \tilde{\mu}}{\rho_1}+\varpi_1)(t-s)} \mathrm{e}^{\tilde{\mu}\beta_1(t-s)} \mathrm{d}s + \int_0^t \tilde{\mu}\zeta \mathrm{e}^{(\frac{\ln \tilde{\mu}}{\rho_1}+\varpi_1)(t-s)} \mathrm{d}s \\ &\leq \frac{\tilde{\mu}\zeta}{-(\frac{\ln \tilde{\mu}}{\rho_1}+\varpi_1) - \tilde{\mu}\beta_1}. \end{aligned} \tag{59}$$

According to Equation (2), and by combining Equations (58) and (59), it will be proven that, for $t > 0$, there is the following inequality

$$v(t) < \zeta e^{-2\rho t} + \frac{\tilde{\mu}\zeta}{-(\frac{\ln\tilde{\mu}}{\rho_1} + \omega_1) - \tilde{\mu}\beta_1} \tag{60}$$

For $t > 0$, Equation (60) will be proved. Thus, if Equation (60) does not hold, $t^* > 0$ exists such that

$$v(t^*) \geq \zeta e^{-2\rho t^*} + \frac{\tilde{\mu}\zeta}{-(\frac{\ln\tilde{\mu}}{\rho_1} + \omega_1) - \tilde{\mu}\beta_1}, \tag{61}$$

and

$$v(t) < \zeta e^{-2\rho t} + \frac{\tilde{\mu}\zeta}{-(\frac{\ln\tilde{\mu}}{\rho_1} + \omega_1) - \tilde{\mu}\beta_1}, t < t^*. \tag{62}$$

According to Equations (58) and (62),

$$\begin{aligned} v(t^*) &\leq \zeta e^{(\frac{\ln\tilde{\mu}}{\rho_1}+\omega_1)t^*} + \int_0^{t^*} e^{(\frac{\ln\tilde{\mu}}{\rho_1}+\omega_1)(t^*-s)}\left[\tilde{\mu}\beta_1 v(s-\tau(s)) + \tilde{\mu}\delta\right] ds, \\ &< e^{(\frac{\ln\tilde{\mu}}{\rho_1}+\omega_1)t^*}\left\{\zeta + \frac{\tilde{\mu}\zeta}{-(\frac{\ln\tilde{\mu}}{\rho_1} + \omega_1) - \tilde{\mu}\beta_1} + \int_0^{t^*} e^{-(\frac{\ln\tilde{\mu}}{\rho_1}+\omega_1)s}\left[\tilde{\mu}\beta_1 v(s-\tau(s)) + \tilde{\mu}\delta\right] ds\right\}. \end{aligned} \tag{63}$$

When $t < t^*$,

$$v(t) < \zeta e^{-2\rho t} + \frac{\tilde{\mu}\zeta}{-(\frac{\ln\tilde{\mu}}{\rho_1} + \omega_1) - \tilde{\mu}\beta_1}, \tag{64}$$

then

$$v(s-\tau(s)) < \zeta e^{-2\rho(s-\tau(s))} + \frac{\tilde{\mu}\zeta}{-(\frac{\ln\tilde{\mu}}{\rho_1} + \omega_1) - \tilde{\mu}\beta_1}, \tag{65}$$

and we have

$$\begin{aligned} v(t^*) &\leq \zeta e^{(\frac{\ln\tilde{\mu}}{\rho_1}+\omega_1)t^*}\left\{\zeta + \frac{\tilde{\mu}\zeta}{-(\frac{\ln\tilde{\mu}}{\rho_1} + \omega_1) - \tilde{\mu}\beta_1}\right. \\ &\left. + \int_0^{t^*} e^{-(\frac{\ln\tilde{\mu}}{\rho_1}+\omega_1)s}\left[\tilde{\mu}\beta(\zeta e^{-2\rho(s-\tau(s))} + \frac{\tilde{\mu}\zeta}{-(\frac{\ln\tilde{\mu}}{\rho_1} + \omega_1) - \tilde{\mu}\beta_1}) + \tilde{\mu}\delta\right] ds\right\} \\ &\leq v(t^*)\zeta e^{(\frac{\ln\tilde{\mu}}{\rho_1}+\omega_1)t^*}\left\{\zeta + \frac{\tilde{\mu}\zeta}{-(\frac{\ln\tilde{\mu}}{\rho_1} + \omega_1) - \tilde{\mu}\beta_1}\right. \\ &\left. + \frac{\tilde{\mu}\zeta\beta_1}{-(\frac{\ln\tilde{\mu}}{\rho_1} + \omega_1 + 2\rho}e^{2\rho\tau_l}\left[e^{-(\frac{\ln\tilde{\mu}}{\rho_1}+\omega_1+2\rho)t^*} - 1\right] + \frac{\tilde{\mu}\delta}{-(\frac{\ln\tilde{\mu}}{\rho_1} + \omega_1) - \tilde{\mu}\beta_1}\left[e^{-(\frac{\ln\tilde{\mu}}{\rho_1}+\omega_1)t^*} - 1\right]\right\} \\ &= \zeta e^{-2\rho t^*} + \frac{\tilde{\mu}\delta}{-(\frac{\ln\tilde{\mu}}{\rho_1} + \omega_1) - \tilde{\mu}\beta_1}. \end{aligned} \tag{66}$$

Obviously, Equation (66) contradicts Equation (61). Then, when $t > 0$, Equation (60) holds. Meanwhile, when $\delta > 0$, according to Equation (52), we have

$$V_1(t) \leq v(t) \leq \zeta e^{-2\rho t^*} + \frac{\tilde{\mu}\delta}{-(\frac{\ln\tilde{\mu}}{\rho_1} + \omega_1) - \tilde{\mu}\beta_1}, t > 0. \tag{67}$$

Letting $\delta \to 0$, according to (66), we have

$$V_1(t) \le v(t) \le \zeta e^{-2\rho t} = \tilde{\mu} \max_{\tau_l \le s \le 0} \{||\psi_1(t)||^2 e^{-2\rho t}\}. \tag{68}$$

Meanwhile, Equation (11) indicates that $V_2(t)$ is continuous for $t \ge 0$. Thus, based on Inequality (48), we have

$$\dot{V}_2(t) \le \varpi_2 V_2(t) + \beta_2 \max_{t-\tau_l \le s \le t} V_2(s) \tag{69}$$

Since $\beta_2 > 0$, it can be deduced from Inequality (26) that $\varpi_2 < 0$. Thus, the conditions mentioned in Lemma 3 are met concerning Equation (68). Then, based on Lemma 3, the initial value in Definition 1, and the Inequalities (49) and (69), we have

$$V_2(t) \le \max_{\tau_l \le s \le 0} ||\psi_2(t)||^2 e^{-\eta t}, t \ge 0, \tag{70}$$

where $\psi_2(t) = (\overline{\psi}_{p+1}^{\mathrm{T}}, \overline{\psi}_{p+2}^{\mathrm{T}}, \ldots, \overline{\psi}_N^{\mathrm{T}})^{\mathrm{T}}$, and η is the unique solution Equation (78).

$$\eta + \varpi_2 + \beta_2 e^{\eta \tau_l} = 0. \tag{71}$$

Combining Inequalities (47)–(48), (67), and (70) and Lemma 3 yields

$$V(t) \le \tilde{\mu} \max_{-\tau_l \le s \le 0} ||\psi_1(t)||^2 e^{-2\rho t} + \max_{-\tau_l \le s \le 0} ||\psi_2(t)||^2 e^{-\eta t} \le (\tilde{\mu}+1) e^{-\mu^* t} \max_{-\tau_l \le s \le 0} ||\overline{\psi}(t)||^2, t \ge 0, \tag{72}$$

where $\mu^* = \min\{2\rho, \eta\}$. Therefore

$$||\epsilon(t)|| \le \sqrt{2(\tilde{\mu}+1)} \max_{-\tau_l \le s \le 0} ||\overline{\psi}(t)|| e^{-0.5\mu^* t}, t \ge 0. \tag{73}$$

Case 2: For $0 < \mu_k^2 < 1$**.**

When $0 < \mu_k^2 < 1$, $\forall k \in N_+$, since $\sup_{k \in N_+} \{t_k - t_{k-1}\} < +\infty$, we have constant ρ_2 satisfying $\rho_2 \ge \sup_{k \in N_+} \{t_k - t_{k-1}\}$.

Similarly, according to Equations (55) and (68), we have

$$W(t) \le e^{\varpi_1 (t-s)} \tilde{\mu}^{(\frac{t-s}{\rho_2}+1)} \le \tilde{\mu}^{-1} e^{(\frac{\ln \tilde{\mu}}{\rho_2} + \varpi_1)(t-s)}, \tag{74}$$

then

$$V_1(t) \le v(t) \le \tilde{\zeta} e^{-2\rho_2 t} = \tilde{\mu}^{-1} \max_{\tau_l \le s \le 0} ||\psi_1(t)||^2 e^{-2\rho_2 t}, t \ge 0. \tag{75}$$

Similarly,

$$V(t) \le \tilde{\mu}^{-1} \max_{-\tau_l \le s \le 0} ||\psi_1(t)||^2 e^{-2\rho_2 t} + \max_{-\tau_l \le s \le 0} ||\psi_2(t)||^2 e^{-\eta t} \le (\tilde{\mu}^{-1}+1) e^{-\mu^* t} \max_{-\tau_l \le s \le 0} ||\overline{\psi}(t)||^2, t \ge 0, \tag{76}$$

where $\mu^* = \min\{2\rho_2, \eta\}$. Therefore

$$||\epsilon(t)|| \le \sqrt{2(\tilde{\mu}^{-1}+1)} \max_{-\tau_l \le s \le 0} ||\overline{\psi}(t)|| e^{-0.5\mu^* t}, t \ge 0. \tag{77}$$

Then, by Definition 1, the coupled memristive neural networks (7) and (8) can achieve global exponential synchronization via the hybrid event-triggered pinning control law (9).

The completion of the proof is shown above. □

Remark 5. *The frequency of the PETS update not only relies on the impulsive instants t_k but also the coupled structure of the system. By utilizing the event-triggered conditions $x(t) \to y(t)$ in*

exponential synchronization, the communication property of CMNNs is automatically satisfied, i.e., one can design distributed triggered conditions for CMNNs so that the information of the PETS can be exchanged among pinned neurons or networks under limited resources. Therefore, the complete PETS (9) considers both the impulse effect and nonidentical property of CMNNs, which indicates that our proposed PETS is more practical than the impulsive controller in [33,34].

Theorem 2. *For the pinning control law (9), considering the error system (11), the impulsive instants, i.e., $t_k(k \in N_+)$, are obtained under the event-triggered condition. Thus, $\rho_1 > 0$ exists such that $\inf\limits_{k\in N_+}\{t_k - t_{k-1}\} > 0$. Thus, the error system can eliminate Zeno behaviors here.*

Proof. For $[t_k, t_{k-1})$, according to Assumption 2, there is

$$\begin{aligned} D^+||e(t)|| &\le ||\dot{e}(t)|| = ||\dot{\epsilon}(t)|| \\ &\le || - \big(D^{**}(t)y_i(t) - D^*(t)x_i(t)\big) + F_A(t) + F_{\Delta A}(t) \\ &+ F_B(t-\tau(t)) + F_{\Delta B}(t-\tau(t)) + \sigma\sum_{j=1}^{N} w_{ij}\Gamma\epsilon_j(t) + \tilde{K}\epsilon(t_{k-1})|| \\ &\le \big[\lambda_{\max}(D^+) + \lambda_{\max}(A^+) + \lambda_{\max}(\tilde{A}^+) + \sigma\lambda_{\max}(W)||\Gamma||\big]||e(t)|| \\ &+ \big[\lambda_{\max}(D^+) + \lambda_{\max}(A^+) + \lambda_{\max}(\tilde{A}^+) + \sigma\lambda_{\max}(W)||\Gamma|| + \lambda_{\max}(\tilde{K})\big]||\epsilon(t_{k-1})|| + ||\Xi||, \end{aligned} \tag{78}$$

where $\tilde{K} = \mathrm{diag}\{|K_1|, |K_2|, \ldots, |K_p|\}$, and $\Xi = \big[2\lambda_{\max}(B^+) + 2\lambda_{\max}(\tilde{B}^+)\big]||M||$.

Then, according to $e(t_{k-1}) = 0$, there is

$$||e(t)|| \le \frac{\Upsilon_1}{\Upsilon_2} \times \big[\exp(\Upsilon_2(t - t_{k-1})) - 1\big], \tag{79}$$

and $\Upsilon_1 = \big[\lambda_{\max}(D^+) + \lambda_{\max}(A^+) + \lambda_{\max}(\tilde{A}^+) + \sigma\lambda_{\max}(W)||\Gamma|| + \lambda_{\max}(\tilde{K})\big]\epsilon(t_{k-1})|| + ||\Xi||$, $\Upsilon_2 = \lambda_{\max}(D^+) + \lambda_{\max}(A^+) + \lambda_{\max}(\tilde{A}^+) + \sigma\lambda_{\max}(W)||\Gamma||$.

Based on the event-triggered condition (30), there is

$$\sqrt{\hbar(\epsilon(t))} \le \frac{\Upsilon_1}{\Upsilon_2} \times \big[\exp(\Upsilon_2(t - t_{k-1})) - 1\big], \tag{80}$$

and $\hbar(\epsilon(t)) = \varepsilon_3|\epsilon^{\mathrm{T}}(t)|\big[\tilde{\alpha} - \varepsilon_1(\lambda_{\max}(B^+))^2 - \varepsilon_2(\lambda_{\max}(\tilde{B}^+))^2 - \varepsilon_3(\lambda_{\max}(\tilde{K}))^2\big]|\epsilon(t)|$.

According to $T_{k-1} = t_k - t_{k-1}$, for $t \in [t_{k-1,t_k})$, $k \in N_+$, there is

$$T_{k-1} \ge \frac{1}{\Upsilon_2}\ln\Big(1 + \frac{\Upsilon_2}{\Upsilon_1}\sqrt{\hbar(\epsilon(t))}\Big). \tag{81}$$

Thus, it can be derived that the lower bound of the inter-execution time exists, and $T_{k-1} = t_k - t_{k-1} > 0$. The error system (11) eliminates the Zeno behavior successfully.

The proof is completed as above. □

Remark 6. *It should be noted that the triggered condition always needs to be detected during the information exchange between the CMNNs. As a result, the self-triggered scheme is formulated to solve this issue. The sampling and pinning control instants can be derived from Equation (81), and the specific process is organized in Algorithm 1 for the self-triggered scheme. It is exhibited that instants of the PETS will not renew until the triggered condition is more exhaustive than the second part of Equation (81).*

Remark 7. *Note that the continuous communication between Systems (7) and (8) is needed for monitoring of the triggered condition (30). As an alternative to event-triggered control schemes, a self-triggered scheme is developed to produce triggered sequences so that the triggered condition shown in (30) does not need to be monitored continuously. Next, based on Theorem 2, the formulation of the self-triggered scheme makes it unnecessary to obtain the state information continuously.*

Clearly, T_{k-1} satisfies Equation (81) all the time. Then, during this inter-execution process, there will be no trigger. To achieve this goal, the subsequent triggered instant should be:

$$\tilde{t}_k = \tilde{t}_{k-1} + \frac{1}{\Upsilon_2}\ln\left(1 + \frac{\Upsilon_2}{\Upsilon_1}\sqrt{\hbar(\epsilon(t))}\right). \tag{82}$$

This paper denotes the update instants for sampling and control as $\tilde{t}_k$, and then this sampling mechanism is represented with self-triggered instants. With a minimum triggered interval, Equation (82) illustrates the calculation of the triggered instants. Note that in this case, there is a possibility that the triggered condition does not hold once the interval in use is larger than the second item within Equation (82).

Theorem 3. *Taking the control law (9) with the error system (11) into consideration, with the self-triggered method, the triggered sequence produced by Equation (82) ensures that the error system can achieve pinning exponential synchronization between Systems (7) and (8). Meanwhile, the error system (11) eliminates Zeno behaviors successfully.*

Proof. For $[t_{k-1}, t_k)$, because the self-triggered instants meet the condition shown in Equation (82), according to Equation (81), $t_k \geq \tilde{t}_k$. Then, the formulation of the event-triggered condition (30) is shown in Equation (82), and it holds for $k \in N_+$. Moreover, considering that the second term involved in Equation (82) satisfies the condition $\frac{1}{\Upsilon_2}\ln\left(1 + \frac{\Upsilon_2}{\Upsilon_1}\sqrt{\hbar(\epsilon(t))}\right) > 0$ all the time, $\tilde{t}_{k-1} < \tilde{t}_k$ holds.

Thus, with the self-triggered mechanism (82), synchronization is realized between Systems (7) and (8) following the pinning control law (9). Moreover, the error system (11) can eliminate the Zeno behavior. The proof is completed. □

3.2. Pinned Nodes Selection

According to [35], $\lambda_1(L_{N-p}) > \alpha/\sigma$ is a common algebraic graph-theoretic criterion for pinning synchronization under the various control methods. Only undirected CMNNs are discussed in this paper, and then the minimal number of nodes will be predicted by analyzing the relationship between $\lambda_1(L_{N-p})$ and $\lambda_{p+1}(L_N)$, to guarantee $\lambda_1(L_{N-p}) > \alpha/\sigma$. The details of the Algorithm 2 are designed as follows:

Algorithm 2 Algorithm for Pinned Nodes' Selection

(1) Suppose that CMNNs are undirected and connected. Assume that there are no empty sets of controlled nodes p. Then, the grounded matrix L_{N-p} (the Laplacian matrix minus the rows and columns of pinned nodes p) is positive definite; that is, the smallest eigenvalue for such a matrix satisfies $\lambda_1(L_{N-p}) > 0$ for $1 \leq p \leq N-1$.
(2) Check whether there exists at least one node that is pinned to make a sufficiently large c that can make $\sigma\lambda_1(L_{N-p}) > \alpha$ (α is a constant that is determined by feedback functions and the inner connecting matrix) to ensure the synchronization of CMNNs. If such nodes exist, go to step (3); otherwise, go to (1).
(3) The minimal number of pinned nodes is chosen by $\lambda_1(L_{N-p}) \leq \lambda_{p+1}(L_N)$ to ensure $\lambda_1(L_{N-p}) > \alpha/\sigma$ by considering the Laplacian spectrum of CMNNs. If satisfied with such a condition, go to step (4); otherwise, re-perform (3).
(4) Consider the degree distribution and step (3); the nodes with larger degrees are chosen as pinned nodes.
(5) According to the PETS and step (4), the convergence time of the error system is calculated. If the convergence time is longer than the previous group, re-perform step (4); otherwise, stop.

4. Numerical Simulations

4.1. Pets for Three Nodes

Here, numerical examples are presented to validate our theoretical results.

This example involves three-dimensional CMNNs, (7) and (8), that consist of three coupled nodes with the edge weights of 1. The system's topology with three nodes is demonstrated in Figure 4a.

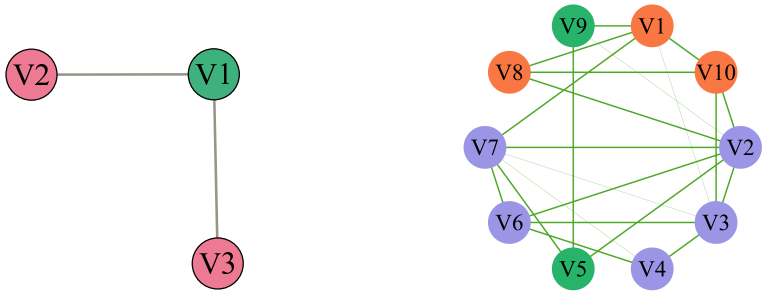

(**a**) (**b**)

Figure 4. The topology structure of CMNNs. (**a**) Topology with 3 nodes. (**b**) Topology with 10 nodes.

For the coupled system, this paper sets the coupling strength $\sigma = 1$. Meanwhile, the inner connecting matrix Γ and coupled matrix W are set as

$$\mathbf{\Gamma} = \begin{pmatrix} 1 & 0 & 0 \\ 0 & 1 & 0 \\ 0 & 0 & 1 \end{pmatrix}, \mathbf{W} = \mathbf{W^S} = (w_{ij})_{3\times 3} = \begin{pmatrix} -2 & 1 & 1 \\ 1 & -1 & 0 \\ 1 & 0 & -1 \end{pmatrix}.$$

For Systems (7) and (8), the time-varying delay is $\tau(t) = e^t/(e^t + 1)$, and it satisfies $\bar{\tau}_l = 0.5$, $\tau_l = 0.25$. $f(\cdot) = \tanh(\cdot)$, and it satisfies Assumptions 1 and 2 with $L_f = 1$, $M_i = 1 (i = 1, 2, 3)$. The values of node x_i are initialized as follows: $\forall s \in [\tau_l, 0]$, $\phi_1(s) = [-1.55, 0.85, 2.12]^{\mathrm{T}}$, $\phi_2(s) = [0.35, -0.98, 0.34]^{\mathrm{T}}$, and $\phi_3(s) = [1.75, -1.15, -2.00]^{\mathrm{T}}$. The initial values of node y_i are as follows: $\varphi_1(s) = [0.82, 2.43, 1.57]^{\mathrm{T}}$, $\phi_2(s) = [0.35, -0.98, 0.34]^{\mathrm{T}}$, and $\phi_3(s) = [1.75, -1.15, -2.00]^{\mathrm{T}}$.

Inspired by [36] and Lemma 4, this paper sets $D = \mathrm{diag}\{1.5, 1.3, 1.2\}$, and the other parameters of Systems (7) and (8) satisfy the condition in Equation (4). We set $\kappa_k = 1$, and then we construct the following matrices of parameters.

$$\mathbf{A}^+ = \begin{pmatrix} 1.8 & 2.8 & 2.9 \\ 1.3 & 1.7 & 1.6 \\ 1.3 & 1.7 & 1.6 \end{pmatrix}, \tilde{\mathbf{A}}^+ = 0.1\sin(t) \begin{pmatrix} 1 & 1 & 1 \\ 1 & 1 & 1 \\ 1 & 1 & 1 \end{pmatrix},$$

$$\mathbf{B}^+ = \begin{pmatrix} 3.8 & 3.0 & 0.9 \\ 0.4 & 0.3 & 0.6 \\ 3.4 & 3.8 & 1.9 \end{pmatrix}, \tilde{\mathbf{B}}^+ = -0.2\cos(t - \tau(t)) \begin{pmatrix} 1 & 1 & 1 \\ 1 & 1 & 1 \\ 1 & 1 & 1 \end{pmatrix}.$$

Within the drive and response system, this paper chooses three different dimensions as phases for the nodes to depict the dynamic trajectory of CMNNs, and the result is shown in Figure 5. It can be seen that the dynamics of CMNNs show chaotic behaviors, and the trajectories of the drive–response systems do not synchronize if the controller is not used.

For the designed pinning event-triggered control scheme (9), this paper chooses node ν_1 as the pinned node, i.e., $N = 3$ and $p = 1$. For the controller, when $\mu_k^2 = 2.25 > 1$, this paper sets $K_1 = 30$, $r = 5$, $\bar{R} = \mathrm{diag}\{5, 0, 0\}$. Then, $\alpha = 0.1$, $\varepsilon_1 = \varepsilon_2 = \varepsilon_3 = 1$, and $\rho_1 = 15$ are chosen to satisfy Theorem 1 and the triggered conditions. By employing Equations (2)–(27), the following results can be obtained

$$\begin{aligned} &\beta = \beta_1 = \beta_2 = 1, \left(\frac{\ln\tilde{\mu}}{\rho_1} + \varpi_1\right) + \tilde{\mu}\beta_1 = -0.2556 < 0, \\ &\Lambda = \varpi_2 + \beta_1 = -8.2255 < 0, \tilde{\alpha} > 450.0536. \end{aligned} \tag{83}$$

When $\mu_k^2 = 0.81 \in (0,1)$, this paper sets $\rho_2 = 15$, and then we have

$$\left(\frac{\ln\tilde{\mu}}{\rho_2} + \varpi_1\right) + \tilde{\mu}^{-1}\beta_1 = -0.5506 < 0. \tag{84}$$

Based on the above parameter setting, we choose the first nodes, i.e., ν_1 as pinned nodes to be controlled. Figure 6 demonstrates in detail the state trajectories. In order to verify the rationality of the proposed theory, we compare different methods and pinned nodes for the designed system. It can be seen from Figure 7 and Table 1, that the expected synchronization is achieved by the CMNNs within the proposed event-triggered pinning control frame (9).

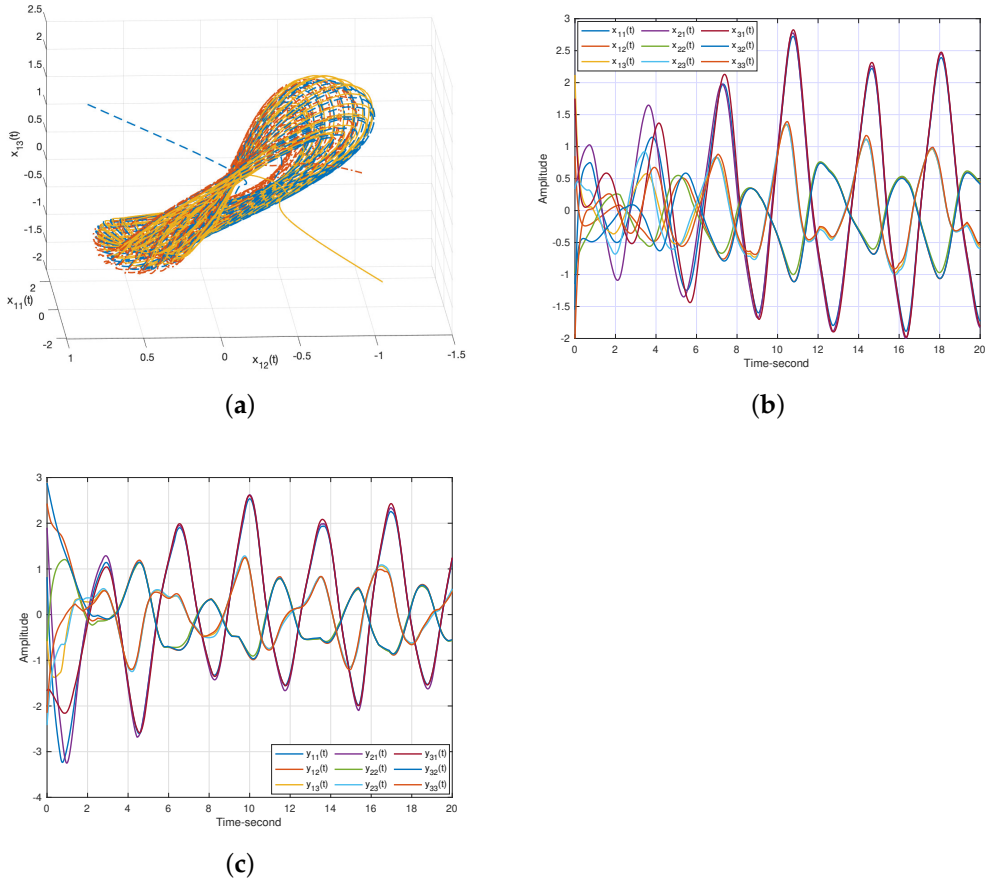

(**a**) (**b**)

(**c**)

Figure 5. The state trajectories produced by Systems (7) and (8) without controller. (**a**) The phase of systems in a complicated space. (**b**) The state curves corresponding to the drive system (7). (**c**) The state curves corresponding to the response system (8).

Different control methods are taken for comparison, and the result is shown in Figure 7 and Table 1. The following observations can be made from different convergence trajectories of synchronization error $e(t)$: (1) It follows from Theorem 1 that Systems (7) and (8) under the control law (9) can achieve synchronization. (2) Under the framework of pinning control, the event-triggered method achieves better performance then the feedback controller, i.e.,

faster convergence with lower energy consumption. The change in the controller and the events of the pinned node are illustrated in Figures 8a and 9.

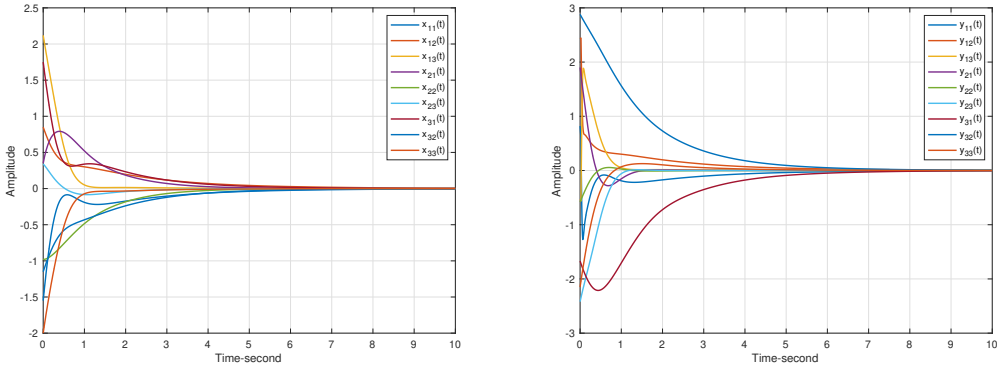

(**a**) (**b**)

Figure 6. The state trajectories produced by Systems (7) and (8) with event triggered pinning control (9). (**a**) State curves of the drive system (7). (**b**) State curves of response system (8).

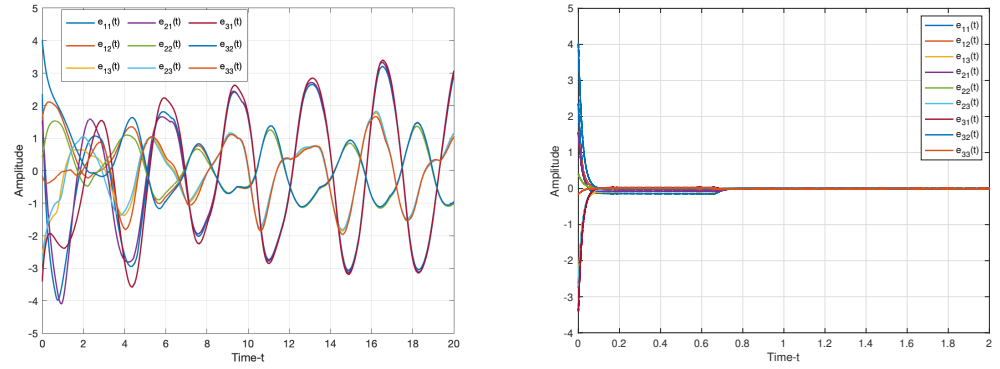

(**a**) (**b**)

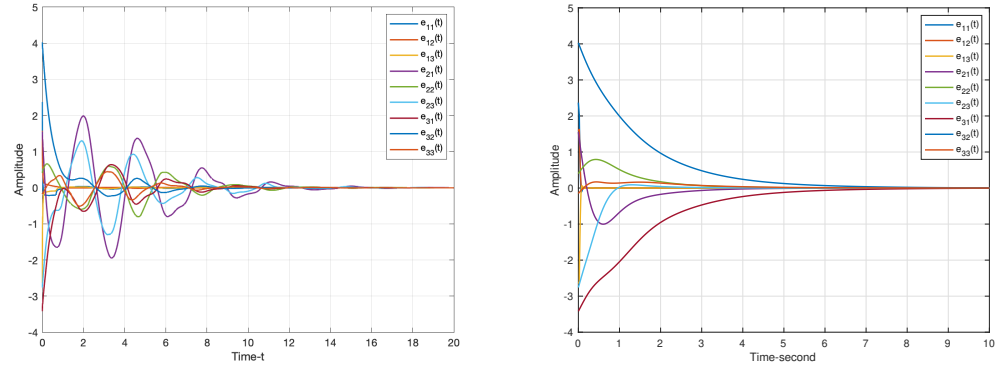

(**c**) (**d**)

Figure 7. Synchronization error trajectories of Systems (7) and (8) with different control methods. (**a**) No controller. (**b**) Feedback controller for all nodes. (**c**) Pinning feedback control for the first node. (**d**) Pinning event triggered control (9) for the first node.

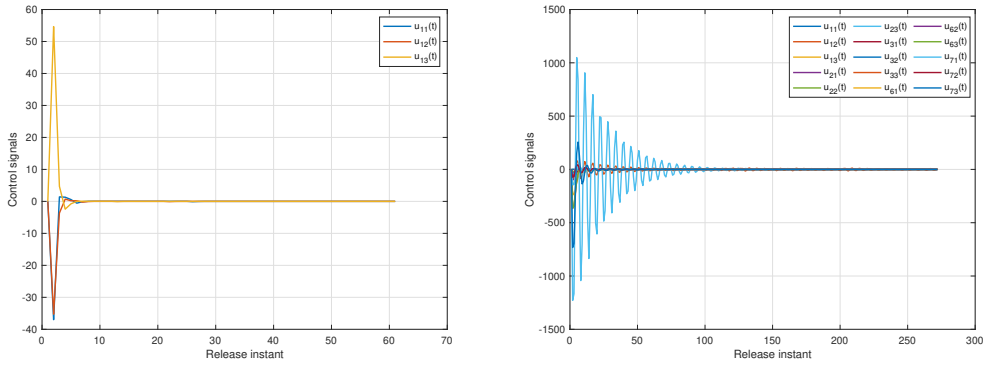

(**a**) (**b**)

Figure 8. Change process of PETS (9). (**a**) For one pinned node $\{v_1\}$. (**b**) For five pinned nodes $\{v_1, v_2, v_3, v_6, v_7\}$.

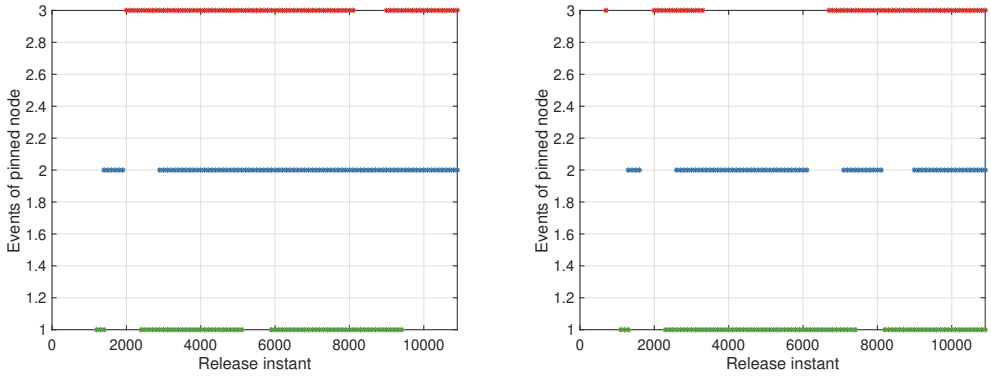

(**a**) (**b**)

Figure 9. Event triggering time instants under PETS (9). (**a**) $\mu_k^2 = 2.25$; (**b**) $\mu_k^2 = 0.81$.

Table 1. Performance comparison of pinning synchronization for convergence.

Control Approach	**None**	**Feedback Control in [37]**		**Our Approach**		
Pinned Nodes	**0**	**All Nodes**	**1**	**Event-Triggered**		**Self-Triggered**
				v_1	v_1, v_2, v_3, v_6, and v_7	v_1
Convergence of system(s)	∞	0.7457	15.867	7.969	1.4687	0.7511

Based on the above parameter setting, it is calculated that $Y_1 = 10.9831$, $Y_2 = 4.3118$, and $T_k > 0$. The calculation results indicate that Theorems 2 and 3 are reasonable. Moreover, the error system (11) successfully eliminates the Zeno behavior. Figure 10a shows that the state trajectories between Systems (7) and (8) converge stably. Figure 10b shows the performance of the designed self-triggered strategy.

Remark 8. *For the self-triggered scheme, Figure 10 and the comparison with Table 2 not only indicate the effectiveness of Theorem 2, but also demonstrate that the self-triggered pinning scheme converges faster than the event-triggered one. The self-triggered approach chooses the smaller triggered interval as the update instant, which leads to a smaller sampling interval and a higher update frequency. Thus, compared with the event-triggered method, the self-triggered synchronization exhibits better performance in convergence. However, it does not fully utilize the limited network bandwidth due to much information exchange taking place.*

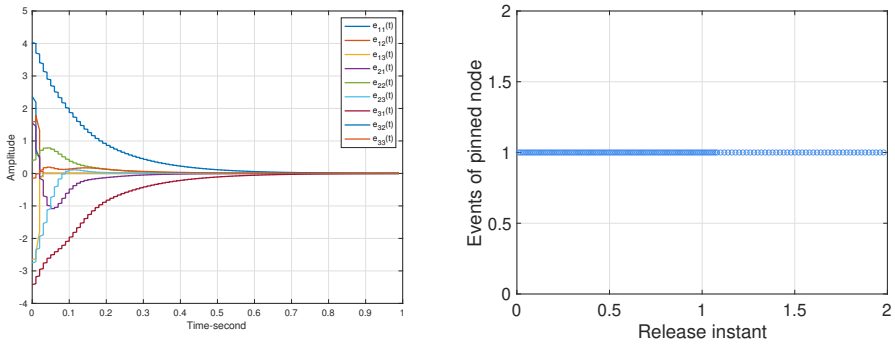

(**a**) (**b**)

Figure 10. The state trajectories produced by Systems (7) and (8) with self triggered pinning control. (**a**) State curves of error system (11). (**b**) Self triggering time instants.

Table 2. Performance comparison of self-triggered scheme.

Self-Triggered	Mean Time Interval			Convergence (s)
	1	2	3	
[38]	0.0546	0.0641	0.0662	8.7435
[5]	0.0746	0.0746	0.0746	2.7184
Theorem 2	0.0158	0.0158	0.0158	0.9032

4.2. PETS for Ten Nodes

Case 1: Pinned Node Selection

Some pinned nodes are selected randomly in some existing approaches on pinning synchronization [39,40]. Nevertheless, when it comes to the event-triggered scheme and uncertain delayed neural networks, schemes on pinning event-triggered synchronization have so far been seldom investigated. Therefore, in this section, inspired by [35,41], Algorithm 1 is selected to choose the nodes that are pinned and to be controlled in Systems (7) and (8).

For Figure 4b, the number of nodes is $N = 10$ and the Laplacian matrix is L_N. Then, all the eigenvalues of L_N are calculated in an increasing order; that is, $\{\lambda_{p+1}(L_N), p = 1, 2, \ldots, 9|7.6561, 7.1368, 6.1810, 5.9315, 1.6720, 1.8704, 4.3112, 3.6205, 3.6205\}$. Then the eigenvalues from $\lambda_1(L_{N-p})$ are derived as $\max_{p=1} \lambda_1(L_9) = 1.7544$, $\max_{p=2} \lambda_1(L_8) = 1.1780$, $\max_{p=3} \lambda_1(L_7) = 1.6114$, $\max_{p=4} \lambda_1(L_6) = 1.6571$, $\max_{p=5} \lambda_1(L_5) = 1.6571$, $\max_{p=6} \lambda_1(L_4) = 1.6972$, $\max_{p=7} \lambda_1(L_3) = 1.6972$, $\max_{p=8} \lambda_1(L_2) = 3.000$, and $\max_{p=9} \lambda_1(L_1) = 5.000$.

Considering the CMNNs shown in Figure 4b, this paper sets the coupling strength $\sigma = 1$. Meanwhile, the inner connecting matrix $\Gamma = \text{diag}\{1, 1, ..., 1\}_{10\times 10}$ and the coupled matrix W is as follows

$$\mathbf{W} = \begin{pmatrix} -5 & 0 & 1 & 0 & 0 & 0 & 1 & 1 & 1 & 1 \\ 0 & -6 & 1 & 0 & 1 & 1 & 1 & 1 & 0 & 1 \\ 1 & 1 & -6 & 1 & 0 & 1 & 1 & 0 & 0 & 1 \\ 0 & 0 & 1 & -3 & 0 & 1 & 1 & 0 & 0 & 0 \\ 0 & 1 & 0 & 0 & -3 & 0 & 1 & 0 & 1 & 0 \\ 0 & 1 & 1 & 1 & 0 & -4 & 0 & 0 & 0 & 1 \\ 1 & 1 & 1 & 1 & 1 & 0 & -5 & 0 & 0 & 0 \\ 1 & 0 & 0 & 0 & 0 & 0 & 0 & -2 & 0 & 1 \\ 1 & 1 & 0 & 0 & 1 & 0 & 0 & 0 & -3 & 0 \\ 1 & 1 & 1 & 0 & 0 & 1 & 0 & 1 & 0 & -5 \end{pmatrix}.$$

As pinned nodes increase from 1 to 9, the trends of $\max_p \lambda_1(L_{N-p})$ and $\lambda_{p+1}(L_N)$ are demonstrated as in Figure 11. According to analysis of Figure 11, it can be seen that $\lambda_{p+1}(L_N)$ stays at greater values than $\max_p \lambda_1(L_{N-p})$ with the increasing number of pinned nodes, and it can predict the small fractional nodes to be controlled. The $\max_p \lambda_1(L_{N-p})$ remains stable since $2 \leq p \leq 7$, which means it is cost-effective to select the number of pinned nodes from 2 to 7.

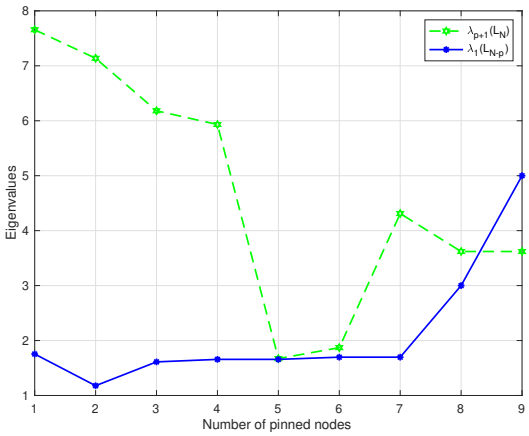

Figure 11. Evolution of $\max_p \lambda_1(L_{N-p})$ and $\lambda_{p+1}(L_N)$ for the increasing of pinned nodes.

Remark 9. *Note that the pinning synchronization of MNNs was adopted in our previous work [37], but the algorithm for pinned node selection was not designed. Inspired by [35], we noticed that* $\max_p \lambda_1(L_{N-p})$ *remains at 1.6 as p increases from 2 to 7, i.e., the percentage of pinned nodes increases from 22.2% to 77.8%. It illustrates that that* $\max_p \lambda_1(L_{N-p})$ *is stable as the number of pinned nodes p increases. This means that the lowest number of pinned nodes* ($2 \leq p \leq 7$) *can be selected since each* $\max_p \lambda_1(L_{N-p})$ *are at the same value. As mentioned above, this paper greatly improves both the applicability of the model and the innovation of the pinning scheme.*

Case 2: Pinning Event-Triggered Synchronization

Taking Algorithm 2 and the Laplace matrix of CMNNs, five nodes are chosen as pinned nodes to be controllers, which satisfies the sufficient conditions of Theorem 1. Therefore, the PETS is a cost-effective method to realize pinning synchronization under uncertain and delayed situations.

For the designed pinning event-triggered control scheme (9), this paper sets $D = \text{diag}\{5.7, 4.6, 3.5, 4.8, 5.9, 4.2, 3.7, 5.5, 3.9, 4.6\}$, and other parameters for Systems (7) and (8) are set as follows

$$\mathbf{A}^+ = \begin{pmatrix} 1.0 & 2.2 & 1.8 \\ 1.0 & 1.0 & 2.4 \\ 0.4 & 0.6 & 1.8 \\ 1.1 & 2.3 & 1.9 \\ 1.2 & 0.9 & 2.3 \\ 0.5 & 0.7 & 1.5 \\ 1.2 & 2.2 & 2.0 \\ 1.3 & 1.0 & 2.4 \\ 0.4 & 0.8 & 1.6 \\ 1.5 & 3.1 & 1.9 \end{pmatrix}, \mathbf{B}^+ = \begin{pmatrix} 3.2 & 0.4 & 1.5 \\ 0.4 & 3.6 & 2.1 \\ 2.6 & 3.2 & 2.6 \\ 3.1 & 0.9 & 1.1 \\ 0.9 & 3.1 & 2.4 \\ 2.1 & 3.4 & 2.5 \\ 3.9 & 1.2 & 1.9 \\ 0.1 & 3.4 & 2.8 \\ 2.5 & 3.3 & 2.7 \\ 3.0 & 0.7 & 1.9 \end{pmatrix}.$$

Figure 12a illustrates the chaotic dynamic behavior of such CMNNs, and Figure 12b shows the rationality of the event-triggered pinning scheme.

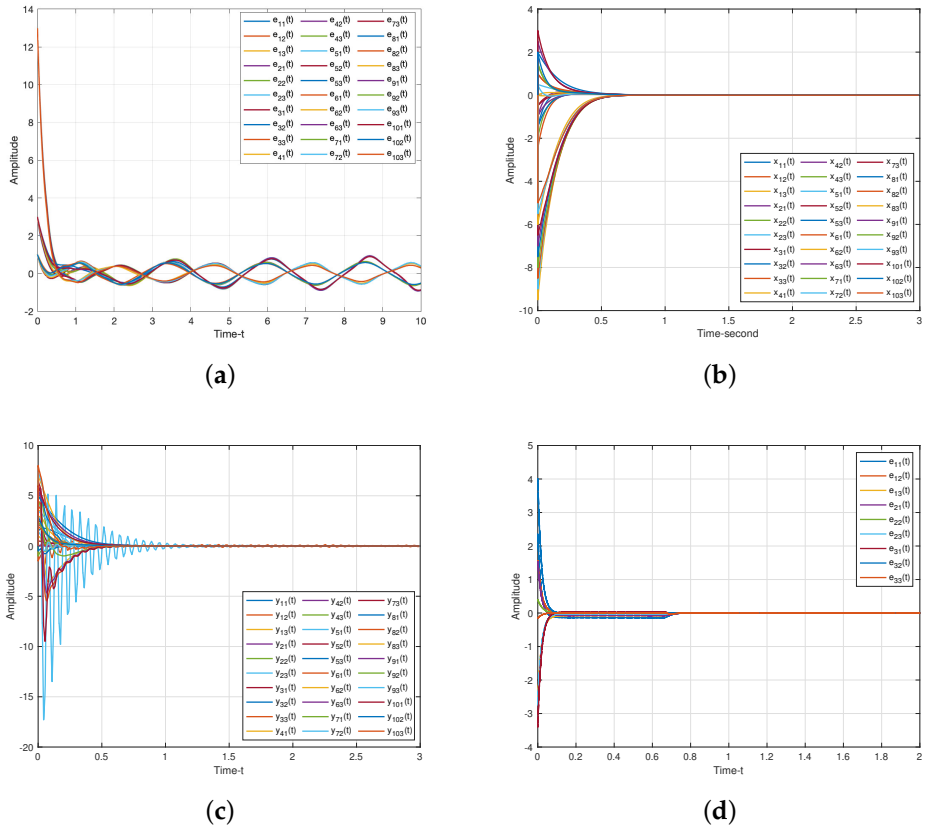

Figure 12. State curves of drive and response systems with 10 nodes. (**a**) States of error system (11) without control. (**b**) States of drive system (7) with PETS (9) on 5 pinned nodes. (**c**) States of drive system (8) with PETS (9) on 5 pinned nodes. (**d**) States of error system (11) with approach (9).

For the controller, when $\mu_k^2 = 2.25 > 1$, this paper sets $k_{11} = 100$, $k_{12} = 100$, $k_{13} = 20$, $k_{21} = 35$, $k_{22} = 20$, $k_{23} = 100$, $k_{31} = 20$, $k_{32} = 38$, $k_{33} = 30$, $k_{61} = 50$, $k_{62} = 80$, $k_{63} = 30$, $k_{71} = 50$, $k_{72} = 80$, $k_{73} = 60$, $r = 5$, and $\bar{R} = \text{diag}\{5, 5, 5, 5, 5, 0, 0, 0, 0, 0\}$. Then, $\alpha = 30$, $\varepsilon_1 = 0.1$, $\varepsilon_2 = 0.005$, $\varepsilon_3 = 1$, and $\rho_1 = 15$, by employing (2)–(27), and the obtained results satisfy Theorem 1 and the triggered conditions. When $\mu_k^2 = 0.81 \in (0, 1)$, this paper sets $\rho_2 = 15$, and we have $\left(\frac{\ln\tilde{\mu}}{\rho_2} + \varpi_1\right) + \tilde{\mu}^{-1}\beta_1 < 0$.

Inspired by [18,35], this paper analyzed the control scheme of pinned node selection in depth. Considering Algorithm 1 and the degree distribution of CMNNs, we choose five nodes as pinned nodes; that is, $\{\nu_1, \nu_2, \nu_3, \nu_6, \nu_7\}$. Table 3 presents the mean time interval of the triggered instants and the convergence time of the error system (11) when the fresh PETS (9) is utilized. Table 3 presents the mean time interval of the triggered instants and the convergence time of the error system (10) when the fresh pinning scheme (43) is used. Figures 8b and 13 demonstrate the information exchange and resource utilization, which confirms the advantages of the proposed method in saving energy and control efficiency.

To investigate whether the control performance is affected by the change in the degree of pinned nodes, this paper replaces the pinned nodes with $\{\nu_1, \nu_2, \nu_3, \nu_4\}$, $\{\nu_3, \nu_6, \nu_9, \nu_{10}\}$, $\{\nu_2, \nu_4, \nu_5, \nu_7\}$, and $\{\nu_5, \nu_7, \nu_8, \nu_9\}$. Then, Figure 14 presents the mean time interval of the error system under the pinning control with four nodes. From the numerical analysis, it can be noticed that when the nodes with less connectivity are pinned, it will make the triggered instants more frequent and lead to more energy consumption. Therefore, the larger connection degree of the pinned nodes will contribute to a better performance of the PETS.

Table 3. Pinned nodes $\{\nu_1, \nu_2, \nu_3, \nu_6, \nu_7\}$ on synchronization.

	ν_{11}	ν_{12}	ν_{13}	ν_{21}	ν_{22}
Maximum Time Interval	0.0877	0.0255	0.9139	0.2133	0.1541
Mean Time Interval	0.0149	0.0149	0.0137	0.0149	0.0137
	ν_{23}	ν_{31}	ν_{32}	ν_{33}	ν_{61}
Maximum Time Interval	0.0255	1.4954	0.1487	0.1496	0.1301
Mean Time Interval	0.0149	0.0149	0.0149	0.0149	0.0137
	ν_{62}	ν_{63}	ν_{71}	ν_{72}	ν_{73}
Maximum Time Interval	0.0255	0.0766	1.4290	0.0350	0.2824
Mean Time Interval	0.0149	0.0149	0.0123	0.0433	0.0147

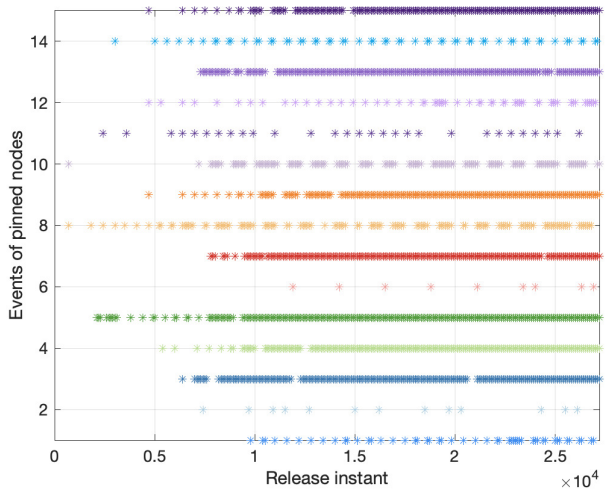

Figure 13. Event triggering time instants for 5 pinned nodes. Different dimensions of pinned nodes correspond to different colors.

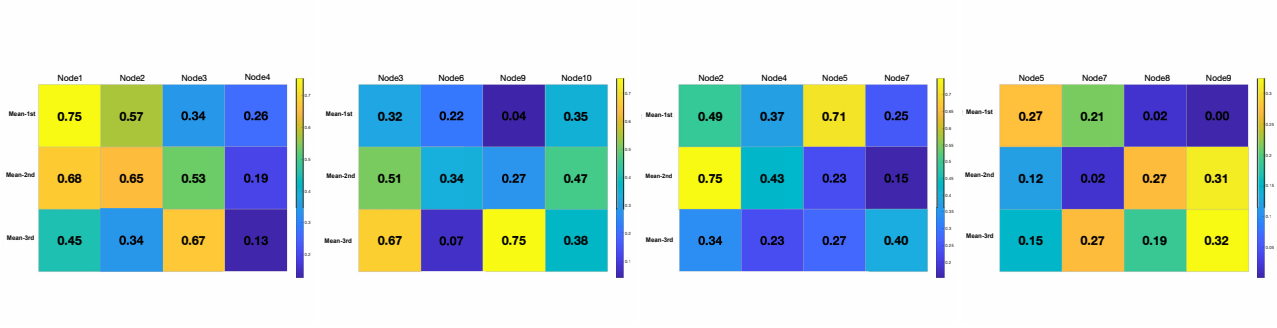

(**a**) (**b**) (**c**) (**d**)

Figure 14. Influence of node selection on convergence. (**a**) $\{\nu_1, \nu_2, \nu_3, \nu_4\}$; (**b**) $\{\nu_3, \nu_6, \nu_9, \nu_{10}\}$; (**c**) $\{\nu_2, \nu_4, \nu_5, \nu_7\}$; (**d**) $\{\nu_5, \nu_7, \nu_8, \nu_9\}$.

Comparing with the current literature [5,42–44], it can be seen that the PETS relies on fewer triggering events from Table 4. Meanwhile, combined with the algorithm of pinned node selection and Theorem 1, it can be seen from Table 2, that our method consumes remarkably less energy for data calculation and detection than other methods. Our proposed method is compared with other advanced works to verify its superiority, and the result is presented in Table 4.

Table 4. Performance comparison of event-triggered scheme.

Event-Triggered	Mean Time Interval			
	1	**2**	**3**	**4**
[5]	0.0198	0.0198	0.0198	-
[42]	0.0127	0.0119	0.0151	-
[43]	0.0114	0.0116	0.0117	0.0046
[44]	0.0153	0.0114	0.0160	0.0214
Theorem 1	0.0467	0.0325	0.0249	-

5. Conclusions

This paper proposed a novel event-triggered pinning control scheme (PETS) for a class of uncertain delayed CMNNs. According to the theory of pinning control schemes and degree distribution of complex neural networks, the algorithm for pinned node selection has been designed. Additionally, taking the pinned nodes into account, a fresh Lyapunov function has been formulated, with a new pinning event-triggered control scheme, a triggered function, an average update interval, and several criteria contrived to guarantee the pinning synchronization for CMNNs. Accordingly, the Zeno behavior could be naturally avoided through the appropriate triggered conditions, which combine the mismatched parameters, nonlinear properties, uncertainties, and the topology of CMNNs. More comparisons indicated that the PETS possessed better energy efficiency and faster stability convergence than other event-triggered approaches.

Author Contributions: Software, W.Z.; formal analysis, M.Y.; investigation, X.B.; writing—original draft, J.F. All authors have read and agreed to the published version of the manuscript.

Funding: This work was supported by the National Natural Science Foundation of China (Grant No. 62106020); Inner Mongolia University high-level talent project (10000-23112101); Inner Mongolia Autonomous Region grassland talent project (1500-242918).

Data Availability Statement: No new data were created or analyzed in this study. Data sharing is not applicable to this article.

Conflicts of Interest: The authors declare no conflicts of interest.

References

1. Cheng, L.; Tang, F.; Shi, X.; Chen, X.; Qiu, J. Finite-time and fixed-time synchronization of delayed memristive neural networks via adaptive aperiodically intermittent adjustment strategy. *IEEE Trans. Neural Netw. Learn. Syst.* **2022**, *34*, 8516–8530. [CrossRef]
2. Liu, F.; Meng, W.; Lu, R. Anti-synchronization of discrete-time fuzzy memristive neural networks via impulse sampled-data communication. *IEEE Trans. Cybern.* **2022**, *53*, 4122–4133. [CrossRef]
3. Yuan, M.; Wang, W.; Wang, Z.; Luo, X.; Kurths, J. Exponential synchronization of delayed memristor-based uncertain complex-valued neural networks for image protection. *IEEE Trans. Neural Netw. Learn. Syst.* **2021**, *32*, 151–165. [CrossRef]
4. Zhu, P.; Cheng, L.; Gao, C.; Wang, Z.; Li, x. Locating multi-sources in social networks with a low infection rate. *IEEE Trans. Netw. Sci. Eng.* **2022**, *9*, 1853–1865. [CrossRef]
5. Wang, W.; Sun, Y.; Yuan, M.; Wang, Z.; Cheng, J.; Fan, D.; Kurths, J.; Luo, X.; Wang, C. Projective synchronization of memristive multidirectional associative memory neural networks via self-triggered impulsive control and its application to image protection. *Chaos Soliton Fract.* **2021**, *150*, 111110. [CrossRef]
6. Cheng, L.; Li, X.; Han, Z.; Luo, T.; Ma, L.; Zhu, P. Path-based multi-sources localization in multiplex networks. *Chaos Soliton Fract.* **2022**, *159*, 112139. [CrossRef]
7. Huang, Y.; Liu, J.; Harkin, J.; McDaid, L.; Luo, Y. An memristor-based synapse implementation using BCM learning rule. *Neurocomputing* **2021**, *423*, 336–342. [CrossRef]
8. Fu, Q.; Zhong, S.; Shi, K. Exponential synchronization of memristive neural networks with inertial and nonlinear coupling terms: Pinning impulsive control approaches. *Appl. Math. Comput.* **2021**, *402*, 126169. [CrossRef]
9. Song, X.; Man, J.; Park, J.H.; Song, S. Finite-time synchronization of reaction-diffusion inertial memristive neural networks via gain-scheduled pinning control. *IEEE Trans. Neural Netw. Learn. Syst.* **2021**, *33*, 5045–5056. [CrossRef] [PubMed]
10. Peng, L.; Li, X.; Bi, D.; Xie, X.; Xie, Y. Pinning multi synchronization of delayed fractional-order memristor-based neural networks with nonlinear coupling and almost-periodic perturbations. *Neural Netw.* **2021**, *144*, 372–383. [CrossRef] [PubMed]

11. Wang, S.; Zhang, Z.; Lin, C.; Chen, J. Fixed-time synchronization for complex-valued BAM neural networks with time-varying delays via pinning control and adaptive pinning control. *Chaos Soliton Fract.* **2021**, *153*, 111583. [CrossRef]
12. Yu, Y.; Zhang, Z.; Zhong, M.; Wang, Z. Pinning synchronization and adaptive synchronization of complex-valued inertial neural networks with time-varying delays in fixed-time interval. *J. Frankl. Inst.* **2022**, *359*, 1434–1456. [CrossRef]
13. Zhou, W.; Sun, Y.; Zhang, X.; Shi, P. Cluster synchronization of coupled neural networks with Lévy noise via event-triggered pinning control. *IEEE Trans. Neural Netw. Learn. Syst.* **2021**, *33*, 6144–6157. [CrossRef]
14. Kashkynbayev, A.; Issakhanov, A.; Otkel, M.; Kurths, J. Finite-time and fixed-time synchronization analysis of shunting inhibitory memristive neural networks with time-varying delays. *Chaos Soliton Fract.* **2022**, *156*, 111866. [CrossRef]
15. Wu, F.; Huang, Y. Finite-time synchronization and $\mathcal{H}_\infty$ synchronization of coupled complex-valued memristive neural networks with and without parameter uncertainty. *Neurocomputing* **2022**, *469*, 163–179. [CrossRef]
16. Huang, Y.; Wu, F. Finite-time passivity and synchronization of coupled complex-valued memristive neural networks. *Inf. Sci.* **2021**, *580*, 775–800. [CrossRef]
17. Zhou, Y.; Zhang, H.; Zeng, Z. Synchronization of memristive neural networks with unknown parameters via event-triggered adaptive control. *Neural Netw.* **2021**, *139*, 255–264. [CrossRef] [PubMed]
18. Zhou, X.; Li, L.; Zhao, X. Pinning synchronization of delayed complex networks under self-triggered control. *J. Frankl. Inst.* **2021**, *358*, 1599–1618. [CrossRef]
19. Zhang, R.; Zeng, D.; Park, J.H.; Liu, Y.; Zhong, S. Pinning event-triggered sampling control for synchronization of T–S fuzzy complex networks with partial and discrete-time couplings. *IEEE Trans. Fuzzy Syst.* **2019**, *27*, 2368–2380. [CrossRef]
20. Wang, X.; Park, J.H.; Yang, H.; Yu, Z. Sampled-data-based $\mathcal{H}_\infty$ fuzzy pinning synchronization of complex networked systems with adaptive event-triggered communications. *IEEE Trans. Fuzzy Syst.* **2021**, *30*, 2254–2265. [CrossRef]
21. Yuan, M.; Luo, X.; Hu, J.; Wang, S. Projective quasi-synchronization of coupled memristive neural networks with uncertainties and impulsive effect. *Front. Neurorobot.* **2022**, *16*, 985312. [CrossRef]
22. Yuan, M.; Luo, X.; Mao, X.; Han, Z.; Sun, L.; Zhu, P. Event-triggered hybrid impulsive control on lag synchronization of delayed memristor-based bidirectional associative memory neural networks for image hiding. *Chaos Soliton Fract.* **2022**, *161*, 112311. [CrossRef]
23. Bao, Y.; Abbas, H.S.; Mohammadpour Velni, J. A learning-and scenario-based MPC design for nonlinear systems in LPV framework with safety and stability guarantees. *Int. J. Control* **2023**. [CrossRef]
24. Bao, Y.; Chan, K.J.; Mesbah, A.; Velni, J.M. Learning-based adaptive-scenario-tree model predictive control with probabilistic safety guarantees using bayesian neural networks. In Proceedings of the 2022 American Control Conference (ACC), Atlanta, GA, USA, 8–10 June 2022; pp. 3260–3265.
25. Feng, J.; Cheng, K.; Wang, J.; Deng, J.; Zhao, Y. Pinning synchronization for delayed coupling complex dynamical networks with incomplete transition rates Markovian jump. *Neurocomputing* **2021**, *434*, 239–248. [CrossRef]
26. Ding, D.; Tang, Z.; Wang, Y.; Ji, Z. Pinning impulsive synchronization of complex networks with multiple sizes of delays via adaptive impulsive intervals. *Circuits Syst. Signal Process.* **2021**, *40*, 4259–4278. [CrossRef]
27. Zhou, Y.; Zeng, Z. Event-triggered impulsive control on quasi-synchronization of memristive neural networks with time-varying delays. *Neural Netw.* **2019**, *110*, 55–65. [CrossRef] [PubMed]
28. Zhang, Y.; Bao, Y. Event-triggered hybrid impulsive control for synchronization of memristive neural networks. *Sci. China Inf. Sci.* **2020**, *63*, 150206. [CrossRef]
29. Wu, T.; Xiong, L.; Cao, J.; Park, J.H.; Cheng, J. Synchronization of coupled reaction-diffusion stochastic neural networks with time-varying delay via delay-dependent impulsive pinning control algorithm. *Commun. Nonlinear Sci. Numer. Simul.* **2021**, *99*, 105777. [CrossRef]
30. Yuan, M.; Wang, W.; Luo, X.; Liu, L.; Zhao, W. Finite-time anti-synchronization of memristive stochastic BAM neural networks with probabilistic time-varying delays. *Chaos Soliton Fract.* **2018**, *113*, 244–260. [CrossRef]
31. Li, X.F.; Fang, J.A.; Li, H.Y. Master–slave exponential synchronization of delayed complex-valued memristor-based neural networks via impulsive control. *Neural Netw.* **2017**, *93*, 165–175. [CrossRef]
32. Zhu, W.; Wang, D.; Liu, L.; Feng, G. Event-based impulsive control of continuous-time dynamic systems and its application to synchronization of memristive neural networks. *IEEE Trans. Neural Netw. Learn. Syst.* **2018**, *29*, 3599–3609. [CrossRef] [PubMed]
33. Jia, Q.; Bram, A.K.; Han, Z. Synchronization of drive-response networks with event-based pinning control. *Neural Comput. Appl.* **2021**, *33*, 8649–8658. [CrossRef]
34. Fu, Q.; Zhong, S.; Jiang, W.; Xie, W. Projective synchronization of fuzzy memristive neural networks with pinning impulsive control. *J. Frankl. Inst.* **2020**, *357*, 10387–10409. [CrossRef]
35. Jin, X.; Wang, Z.; Yang, H.; Song, Q.; Xiao, M. Optimizing pinning control of complex dynamical networks based on spectral properties of grounded Laplacian matrices. *IEEE Trans. Syst. Man Cybern. Syst.* **2018**, *51*, 786–796. [CrossRef]
36. Yang, Z.; Zhao, B.; Liu, D. Synchronization of Delayed Memristor-Based Neural Networks via Pinning Control With Local Information. *IEEE Trans. Neural Netw. Learn. Syst.* **2023**. [CrossRef] [PubMed]
37. Yuan, M.; Luo, X.; Wang, W.; Li, L.; Peng, H. Pinning synchronization of coupled memristive recurrent neural networks with mixed time-varying delays and perturbations. *Neural Process. Lett.* **2018**, *49*, 239–262. [CrossRef]
38. Wang, W.; Wang, C.; Guo, Y.; Luo, X.; Gao, Y. Self-triggered consensus of vehicle platoon system with time-varying topology. *Front. Neurorobot.* **2020**, *14*, 53. [CrossRef]

39. Shi, L.; Zhang, C.; Zhong, S. Synchronization of singular complex networks with time-varying delay via pinning control and linear feedback control. *Circuits Syst. Signal Process.* **2021**, *145*, 110805. [CrossRef]
40. Jin, X.; Wang, Z.; Yang, H.; Song, Q.; Xiao, M. Synchronization of multiplex networks with stochastic perturbations via pinning adaptive control. *J. Frankl. Inst.* **2021**, *358*, 3994–4012. [CrossRef]
41. Liu, X.; Tay, W.P.; Liu, Z.W.; Xiao, G. Quasi-synchronization of heterogeneous networks with a generalized Markovian topology and event-triggered communication. *IEEE Trans. Cybern.* **2019**, *50*, 200–4213. [CrossRef]
42. Yang, Y.; Yue, D.; Dou, C. Output-based event-triggered schemes on leader-following consensus of a class of multi-agent systems with Lipschitz-type dynamics. *Inf. Sci.* **2018**, *459*, 327–340. [CrossRef]
43. Liu, J.; Wu, H.; Cao, J. Event-triggered synchronization in fixed time for complex dynamical networks with discontinuous nodes and disturbances. *J. Intell. Fuzzy Syst.* **2020**, *38*, 2503–2515. [CrossRef]
44. Liu, L.; Zhou, W.; Li, X.; Sun, Y. Dynamic event-triggered approach for cluster synchronization of complex dynamical networks with switching via pinning control. *Neurocomputing* **2019**, *340*, 32–41. [CrossRef]